

UNCLASSIFIED  
~~RESTRICTED~~

Copy

6

RM A9K02b

CLASSIFICATION CHANGED

To UNCLASSIFIED

~~RESTRICTED~~  
**NACA**

~~761~~  
C.2

By authority of *H. L. Dryden* Date *6-11-53*

*per NACA Release form #1513 By HLR, 7-20-53*  
**RESEARCH MEMORANDUM**

A DESIGN STUDY OF LEADING-EDGE INLETS

FOR UNSWEPT WINGS

By Robert E. Dannenberg

Ames Aeronautical Laboratory  
Moffett Field, Calif.

CLASSIFIED DOCUMENT

This document contains classified information affecting the National Defense of the United States within the meaning of the Espionage Act, USC 2381 and 2382. Its transmission or the revelation of its contents in any manner to an unauthorized person is prohibited by law. Information so classified may be imparted only to persons in the military and naval services of the United States, appropriate civilian officers and employees of the Federal Government who have a legitimate interest therein, and to United States citizens of known loyalty and discretion who of necessity must be informed thereof.

~~RESTRICTED~~  
LANCET  
JUN 30 1950

**NATIONAL ADVISORY COMMITTEE  
FOR AERONAUTICS**

WASHINGTON  
June 30, 1950

~~RESTRICTED~~  
UNCLASSIFIED

UNCLASSIFIED

NACA RM A9K02b



NATIONAL ADVISORY COMMITTEE FOR AERONAUTICS

RESEARCH MEMORANDUM

A DESIGN STUDY OF LEADING-EDGE INLETS  
FOR UNSWEPT WINGS

By Robert E. Dannenberg

SUMMARY

A practical method, employing a lofting technique, is presented for determining the profile coordinates of an air inlet for the leading edge of an airfoil from formulas which are dependent only on the airfoil coordinates and on the height of the opening. The usefulness of this method is demonstrated by an analysis of the results of a wind-tunnel investigation of leading-edge inlets in an airfoil having the NACA 63<sub>1</sub>-012 section. The analysis indicates that satisfactory characteristics were obtained for this airfoil with inlets designed from the formulas. The analysis includes a study of the effects of variations of inlet geometry on the experimentally determined aerodynamic characteristics of the ducted airfoil.

It was found during the course of the investigation that the base-profile concept of thin-airfoil theory could be applied to a ducted airfoil with satisfactory results. With a given inlet and its experimental velocity distribution as a reference, the change in the velocity distribution caused by a change in inlet profile was calculated and the results agreed well with experiment. A numerical example is included in the appendix.

INTRODUCTION

Previous studies of wing leading-edge inlets have been confined, in general, to thick wings and to applications where relatively small amounts of air were to be supplied to installations such as radiators or carburetors. References 1 through 3 have shown by results of experiment that the problem with a leading-edge inlet in a thick wing (18-percent) is mainly that of obtaining high pressures at the entrance to the cooler or to the carburetor. The effect of the inlet on the maximum lift was small. With a 15-percent-thick wing (reference 4), the influence of the inlet design on the maximum lift was greater. Additional data are available for

~~RESTRICTED~~

UNCLASSIFIED

leading-edge inlets in relatively thick wings (15- to 18-percent) for radiator applications where air flowing through the wing is exhausted from the surface of the wing (references 5 through 9) or at the trailing edge of the wing (references 10 through 12).

Theoretical treatments of the problem of wing leading-edge inlets in references 13 and 14 have been concerned with two-dimensional airfoils with inlets at the leading edges and outlets at the trailing edges. In reference 13, the velocity distribution over the inlet section is calculated by a method of conformal mapping which is intricate and laborious. Reference 14 is concerned with the exact form of symmetrical inlets for uniform velocity distribution. The resulting inlet lips are impractically thin. Another type of theoretical development, given in references 15 and 16, deals with a symmetrical shape with outer surfaces which extend to infinity. The shapes of inlets derived by the methods proposed in the latter two references are not readily adaptable to conventional airfoil sections.

With the use of jet engines in conjunction with leading-edge inlets in thin wings (10- to 14-percent), it is desirable to increase the ratio of the inlet height to the section thickness over that used in the previously mentioned references. The design of such inlets can have critical effects on the aerodynamic characteristics of the wings. In addition, the design of the inlet affects the performance of the engine through, mainly, its effect on the magnitude of the ram-pressure recovery. Little information other than results of tests of inlets for specific airplanes of the armed services has been available on the design of leading-edge inlets for jet engines.

The investigation discussed in this report was undertaken to provide a practical means of designing inlets to fit into the leading edges of straight or slightly tapered wings and to evaluate the effects of variations of the inlet geometry and of the velocity of the entering flow. This report presents the development of formulas for specifying the profile coordinates for leading-edge inlets, the experimental results for such inlets in an airfoil having the NACA 63<sub>1</sub>-012 section, and an application of thin-airfoil theory to the calculation of the aerodynamic effects of changes to the profile of the inlets. The majority of the inlet shapes tested were designed from the formulas. The inlet profiles considered differed widely in entrance height, in upper-lip radius, in stagger of the lips, and in external chordwise profile. The shape of the internal duct was considered to be beyond the scope of the investigation because of its dependence on the type of installation.

#### SYMBOLS AND COEFFICIENTS

The symbols which indicate geometric properties of the plain and ducted airfoil sections are shown in figure 1. All geometric symbols are in percent of the chord.

- A distance from origin of upper-lip leading-edge radius to chord line
- B distance from origin of lower-lip leading-edge radius to chord line
- c airfoil chord length
- $C_D$  external drag coefficient (excluding inlet internal drag), based on airfoil area
- $\Delta C_D$  external increment of drag coefficient caused by inlet, based on airfoil area
- $C_L$  lift coefficient based on airfoil area
- $C_{m_c}/4$  pitching-moment coefficient about quarter-chord line based on airfoil area and airfoil chord
- d inlet entrance height
- h distance perpendicular to chord line
- H total pressure, pounds per square foot
- $\frac{H_1 - p_o}{H_o - p_o}$  ram-recovery ratio
- $M_{cr}$  critical Mach number
- p static pressure, pounds per square foot
- P pressure coefficient  $\left( \frac{p_l - p_o}{q_o} \right)$
- q dynamic pressure, pounds per square foot
- r inlet lip radius
- R airfoil leading-edge radius
- S distance parallel to chord line from leading edge of upper lip to leading edge of lower lip of staggered inlet.
- t maximum thickness of airfoil section
- v local velocity over symmetrical airfoil at zero angle of attack (See reference 17.)

$\Delta v$	increment of local velocity caused by addition of camber (See reference 17.)
$\Delta v_a$	increment of local velocity caused by additional load distribution associated with angle of attack (See reference 17.)
$v_b$	local velocity over ducted airfoil at zero angle of attack
$\Delta v_1$	increment of local velocity caused by change in inlet-velocity ratio
$\Delta v_s$	increment of local velocity caused by change in external coordinates of inlet
$V$	velocity, feet per second
$V_1/V_0$	inlet-velocity ratio
$x$	distance along chord from leading edge
$x^*$	distance along chord from leading edge for inlet with stagger
$X$	distance along chord from leading edge to station of maximum airfoil thickness
$y_D$	external ordinate of inlet section, measured perpendicularly from line through origin of lip radius parallel to chord line
$y_w$	ordinate of airfoil section, measured perpendicularly from chord line
$\Delta y_D$	increment of external ordinate of inlet section
$Y$	maximum external ordinate of inlet section at station $X$ , measured perpendicularly from line through origin of lip radius parallel to chord line
$\alpha$	angle of attack of airfoil chord line, degrees
$\beta$	largest acute angle between chord line and line normal to the upper surface that passes through origin of leading-edge radius, degrees
$\phi$	stagger (acute angle between line normal to chord line and line joining origins of upper- and lower-lip radii), degrees

The following subscripts are used in conjunction with the above symbols and coefficients:

o free stream

l	local
L	lower
u	uncorrected
U	upper
1	in duct inlet at rake station (5 percent of chord behind leading edge)

#### DERIVATION OF INLET PROFILE

A leading-edge inlet designed by the method presented in this report entails a change in the profile of the airfoil from the leading edge to the station of maximum airfoil thickness. Behind the latter station the shape of the airfoil remains unchanged. The method for determining the profile for an inlet in an airfoil is presented in two parts, designated as design step 1 and design step 2. Design step 1 provides a method for the design of a leading-edge inlet of arbitrary height, upper- and lower-lip radii, and stagger for a symmetrical airfoil. Design step 2 is concerned primarily with an alteration of the profile determined by step 1 to improve the internal pressure-recovery characteristics at high angles of attack.

#### Design of Inlets for Symmetrical Airfoils

Design step 1.— In developing a leading-edge inlet for a symmetrical airfoil (fig. 1(a)), the inlet lips can be considered as the forward portions of the upper and lower halves of the airfoil with the maximum ordinates decreased from  $t/2$  to  $Y$ . The lip sections are considered to extend from the leading edge to the station of maximum thickness. The upper-lip profile (fig. 1 (b)) is derived by an affine transformation from the original airfoil section as follows: The lip ordinates are calculated by reducing the airfoil ordinates in proportion to the thickness ratio  $\frac{Y}{t/2}$ . The upper-lip radius is assumed to vary as the square of the thickness ratio. The values of the upper-surface ordinates and of the upper-lip radius are thus obtained from

$$y_{DU} = y_w \left( \frac{Y}{t/2} \right) \quad (1)$$

and

$$r_U = R \left( \frac{Y}{t/2} \right)^2 \quad (2)$$

On the basis of the notation of figure 1, the maximum airfoil thickness can be expressed as

$$t = d + r_U + r_L + 2Y \quad (3)$$

Test results have shown that a lower-lip radius of about one-half the upper-lip radius calculated from equation (2) is, in general, satisfactory. With a lower-lip radius equal to one-half that of the upper lip, the maximum airfoil thickness is

$$t = d + \frac{3}{2} r_U + 2Y \quad (4)$$

Substituting equation (2) into equation (4) and solving for  $Y$  yields

$$Y = \frac{-t^2 + t \sqrt{t^2 - 6R(d-t)}}{6R} \quad (5)$$

whereas, if equation (3) is used in place of equation (4),

$$Y = \frac{-t^2 + t \sqrt{t^2 - 4R(d+r_L-t)}}{4R} \quad (6)$$

Substituting this value of  $Y$  in equation (1) will produce ordinates which fair smoothly into the upper-lip radius determined from equation (2) and into the airfoil profile at the maximum thickness. The inner surface of the lip is formed by a line tangent to the circle of radius  $r_U$  and parallel to the chord line. Ordinates calculated by use of equation (5) are dependent only on the inlet entrance height for a given airfoil section.

The leading edge of the lower lip is located in the same plane as that of the symmetrical airfoil as indicated in figure 1(b). In order that the external ordinates fair smoothly into the smaller lower-lip radius, the ordinates from equation (1) are reduced linearly. The reduction in the lower-lip ordinates is obtained from

$$\Delta y_D = \sin \beta (r_U - r_L) \left(1 - \frac{x}{X}\right) \quad (7)$$

The value of  $\beta$  is measured from the profile of the symmetrical airfoil as shown in figure 1(c). The external ordinates of the lower lip are then

$$y_{D_L} = y_{D_U} - \Delta y_D \quad (8)$$

Using a linear reduction of ordinates in this manner introduces a small change in the first derivative ( $dy/dx$ ) at the position of maximum thickness. However, this change is so small that it may be ignored. The inner surface of the lip is formed by a line tangent to the circle of radius  $r_L$  and parallel to the chord line. Equations (7) and (8) can also be used to calculate the change in ordinate resulting from an increase or decrease in the upper-lip radius compared to the design value of equation (2).

The leading edges of the upper and lower lips of the inlet designed in the foregoing manner lie in the same plane as the leading edge of the plain airfoil. Locating the leading edge of the lower lip behind the leading-edge location of the plain airfoil introduces stagger into the inlet profile. The angle of stagger is shown in figure 1(d). The ordinate stations for the staggered lower lip can be calculated by a linear change in chordwise location from a value of  $S$  (fig. 1(d)) at the leading edge to zero at the maximum thickness. While the values of lip radius and the ordinates remain unchanged, the modified chordwise stations are

$$x' = x + S \left( \frac{Y - x}{X} \right) \quad (9)$$

Design step 2.— The results of tests with inlets designed from step 1 indicated that the shape of the inner surface of the lower lip was the main factor contributing to an abrupt reduction in ram-pressure recovery at small angles of attack. When the lower surface is lowered and rounded, as shown in figure 1(e), the angle-of-attack range for maximum ram-pressure recovery was increased. For a given entrance height, this change permits the addition of a greater amount of camber, or droop, to the upper lip than would be attainable if the lower lip from design step 1 were left unaltered. For a practical amount of stagger, the upper-lip camber permissible with the lower lip unaltered is so limited that its aerodynamic contributions are negligible.

The coordinates of an inlet with a rounded inner surface of the lower lip and a drooped upper lip can be determined as follows: The distance from the origin of the lower-lip radius to the airfoil chord line is increased by an amount  $h_L$  as shown in figure 1(e). The optimum value of  $h_L$  varies with the amount of lower-lip stagger. With  $20^\circ$  stagger, values from one-half to three-fourths times the lower-lip radius are recommended. With  $40^\circ$  stagger, values from one to one-and-one-half times the lower-lip radius are recommended. The maximum external ordinate of the lower lip is reduced to a value  $Y - h_L$ . The external ordinates are calculated from the values given in equation (8) by the relation

$$\left( Y_{D_L} \right)_{\text{step 2}} = \left( \frac{Y - h_L}{Y} \right) Y_{D_L} \text{ step 1} \quad (10)$$

The inner surface of the lower lip is joined to the internal duct at a station 2 to 5 percent of the chord behind the lip leading edge. A parabolic curve is used in fairing this section of the lip (fig. 1(e)).

As a result of the staggering and rounding of the lower lip, it is necessary to droop the upper lip in order to maintain a constant ratio of  $d/t$ . To do this, the distance between the origin of the upper-lip radius and the chord line is reduced by an amount  $h_U$  as shown in figure 1(e). The value of  $h_U$  is determined by fairing the inner surface of the upper lip so that the mean perpendicular height between the inner surfaces of the inlet is reduced to the original inlet opening height. It is recommended that the inner surface of the upper lip join the circle of radius  $r_U$  tangentially at a point in which the radius is in a position approximately normal to the chord line. If a linear reduction of ordinate were used as in equations (7) and (8), the change in ordinate caused by the droop of the upper lip would introduce a significant discontinuity in the first derivative ( $dy/dx$ ) at the position of maximum thickness. To insure a smooth surface and a uniform first derivative, the external lip ordinates which follow from the new lip-radius location are determined as follows: A mean line is selected from reference 17 having a maximum ordinate at the same chordwise station as that of the plain airfoil. The mean-line ordinates from the leading edge to the maximum thickness are expressed as fractions of the maximum mean-line ordinate. These values are subtracted from 1.0, multiplied by the value of  $h_U$ , and finally subtracted from the upper-lip ordinate  $y_{PU}$  at each station. The resulting upper lip is shown in figure 1(e).

The foregoing method (steps 1 and 2) permits the determination of the chordwise profile coordinates for the ducted airfoil section. The design of the internal contour behind the 2- to 5-percent-chord stations is dependent upon the type of installation and is beyond the scope of this report. Means of fairing the inlet shape into the airfoil in the spanwise direction are considered in the section Discussion under the heading End-Closure Shape.

#### Design of Inlets for Cambered Airfoils

In developing an inlet for a cambered airfoil, the camber is first removed to obtain the coordinates of the corresponding symmetrical airfoil section. The inlet is designed for the symmetrical section by design steps 1 and 2. The ordinates thus calculated and measured from the chord line of the symmetrical airfoil section are combined normal to the mean line of the cambered airfoil section by the method given in reference 17 to obtain the inlet coordinates for the cambered airfoil section.

#### APPARATUS AND TESTS

To study the characteristics of inlets derived from the design method, an airfoil with various leading-edge inlets was mounted in one of the Ames

7- by 10-foot wind tunnels so that the span of the airfoil extended across the 7-foot dimension of the test section as indicated in figure 2(a). The airfoil had the NACA 63<sub>1</sub>-012 section and a constant chord of 4.0 feet. The removable inlet section covered the central 19.6 percent of the airfoil span. All inlets were mounted in the same relative spanwise position on the airfoil. To facilitate model changes, a simple type of end fairing was used during most of the investigation as shown in figure 2(b). An inlet with a recommended end-closure shape is shown in figure 2(a).

Air was drawn through the inlets into a hollow spar in the airfoil and then through a ducting system by a compressor outside the test chamber. A mercury seal isolated the model and the scale system from the mechanical forces that would otherwise have been imposed by the external ducting. The quantity of air flowing through the inlet was calculated from the pressure drop across a calibrated orifice plate. The inlet pressure losses were measured by a rake of total- and static-pressure tubes 5 percent of the chord behind the leading edge. The rake was normal to the chord line at the center of the inlet. The arithmetic mean of the rake-tube pressure measurements was used to calculate the ram-recovery ratio. The pressure distribution over the external surfaces of the inlets was measured by orifices that were flush with the surfaces and were connected to multiple-tube manometers, the readings of which were photographically recorded.

Tunnel-wall corrections to the force measurements were applied according to the methods discussed in reference 18 by the following equations:

$$\alpha = \alpha_u + 0.303 C_{L_u}$$

$$C_L = 0.953 C_{L_u}$$

$$C_D = 0.9795 C_{D_u}$$

The test results are presented for a Mach number of 0.14 and a Reynolds number of 3,840,000 based on the airfoil chord.

The external drag of each inlet was computed by subtracting the drag of the airfoil without inlet and the drag of the internal-flow system from the total drag as measured by the wind-tunnel scale system. The internal drag was computed by the method given in reference 19 based on measurements of the quantity of air flowing through the inlet. It may be seen readily that as the airfoil and internal drag forces are large in comparison with the total drag force, any inaccuracy in measurement appears as a large proportion of the external drag force. In order to reduce this error to a minimum, particular care was taken in making all drag measurements; the accuracy of the inlet external-drag coefficients is within  $\pm 0.0002$ .

## RESULTS OF EXPERIMENTS

The leading-edge inlets tested are designated as either design inlets or modified inlets. Pertinent information for the determination of the coordinates of the individual lips tested are presented in table I.

The design inlets were derived by the procedure given in design steps 1 and 2. A lower-lip radius of 0.30 percent of the airfoil chord was selected for all inlets of the investigation. The aerodynamic characteristics of the plain airfoil are given in figure 3, while those of the airfoil with the design inlets are presented in figures 4 to 16 for the following geometric arrangements:

d/t	Stagger (deg)
0.15	0, 20
.20	0, 20, 40
.25	0, 20, 40
.30	20

The design inlets were modified in two different ways. The first type of modification consisted of reducing the upper-lip radius below the design radius and determining the lip ordinates from equations similar to equations (7) and (8). The aerodynamic characteristics of the airfoils with this type of lip modification are given in figures 10(b), 11(b), 17, 18, and 19. A second type of modification to the design inlets consisted of varying the ordinates above and below the design values by use of a conic lofting procedure that altered the inlet profile and maintained smooth curves. The lip radii remained unchanged during those modifications. The pressure distributions on the second type of modified lips are shown in figures 20 and 21.

## DISCUSSION

In the application of the test results to the design of inlets, the conditions under which the data were obtained must be taken into account. Specifically, with the addition of an inlet to the airfoil, the flow over the entire span of the airfoil was no longer two-dimensional as the inlet section extended over approximately one-fifth of the span. Thus the data are representative of the airfoil characteristics and should not be construed as section characteristics.

## Design Inlets

Lift and moment.— The lift-coefficient variation with the angle of attack of the unducted airfoil is shown in figure 3, while the variation for the airfoil with the design inlets is given in figures 4, 6, 8, and 10. In the latter figures, the experimental values of lift coefficient are shown for the lowest value of inlet-velocity ratio to give maximum lift. Inspection of the lift curves reveals that the maximum lift coefficient of the airfoil with any of the design inlets for zero internal flow was less than that of the airfoil without the inlet. Increasing the inlet-velocity ratio increased the maximum lift coefficient until values equal to that for the plain airfoil were obtained. Further increase in the inlet-velocity ratio did not increase the maximum lift. As shown in figure 12, increasing the inlet entrance height or the amount of stagger increased the inlet-velocity ratio necessary for obtaining a maximum lift equivalent to that of the plain airfoil. The inlets did not change the lift-curve slope appreciably. The pitching-moment characteristics of the airfoil with the inlets are not presented as no changes in the moments were noted when compared to those of the plain airfoil other than those associated with the loss in lift at low inflow rates.

The loss of maximum lift encountered with small inflow would not be detrimental during normal operation for an airplane using a leading-edge inlet for supplying air to a jet engine. For unaccelerated flight near maximum lift, the inlet-velocity ratio would be greater than unity and the lift provided by the inlet section would be equivalent to that of the section without the inlet. In case of an engine failure or a power-off landing, however, the loss of maximum lift associated with low inflow would be critical. A by-pass system may be necessary to forestall this reduction of maximum lift.

External drag.— The drag characteristics of the airfoil with and without a design inlet were determined from the tunnel-scale measurements. The difference between the results was considered to represent the increment in external drag coefficient caused by the addition of an inlet to the airfoil. These incremental values for the various design inlets were found to be independent of the entrance height and are, therefore, presented in figure 13 as a single curve for a given inlet-velocity ratio and angle of stagger for stagger angles of  $0^\circ$ ,  $20^\circ$ , and  $40^\circ$ . Inspection of the figure indicates that the external drag increments due to the inlets are small. The positive drag increments for an angle of attack of  $0^\circ$  and an inlet-velocity ratio of zero can probably be attributed to an increase of pressure drag due to the addition of the inlet, together with a forward movement of the position of transition from laminar to turbulent flow in the boundary layer. The reduction of the external-drag increment with increasing angle of attack and inlet-velocity ratio may be associated with several factors, such as (1) changes in the pressure drag over the ducted section of the span, (2) changes in the spanwise distribution of

load, (3) changes in the localized "bubble" of separated flow near the leading edge along the part of the span occupied by an inlet, and (4) changes in the position of transition.

Ram-pressure recovery.— The ram-recovery ratios for the design inlets are shown as functions of the angle of attack in figures 4, 6, 8, and 10. Inspection of these figures indicates that for the unstaggered inlets there were sharp reductions in the ram-recovery ratio at low angles of attack. Stagger increased the angle-of-attack range for complete pressure recovery. In addition, the severity of the reduction in the ram-pressure recovery with increasing angle of attack was lessened by the increased lip stagger.

The effects of changes of lower-lip shape on the ram-recovery ratio and on the pressure distribution over the outer surface of the lower lip are shown in figure 14 for an inlet with a nominal ratio of entrance height to maximum airfoil thickness of 0.15 and a lip stagger of  $20^\circ$ . The results for the lower lip developed from design step 1 are shown in figure 14(a). This lip resulted in poor ram-pressure recovery. By drooping and rounding the inner surface of the lower lip (design step 2) as noted in figure 14(b) and particularly in figure 14(c), the angle-of-attack range for maximum ram-pressure recovery was increased considerably. Rounding the inner surface of the lower lip not only delayed the internal-flow separation to a higher angle of attack, but also reduced the effect of inlet-velocity ratio on the ram-pressure recovery. The effect of a change in the upper-lip radius on the recovery characteristics of the inlet was only slight, as indicated by a comparison of the results for the inlet with a design upper-lip radius (fig. 4(c)) with the results for a modified lip radius (fig. 14(b)).

A change to the inner-lip contour, as indicated in figure 14, may also be considered as a change in the inclination of the axis of the internal-flow system. The angle of inclination of the inlet shown in figure 14(c) measured  $9.5^\circ$ . The effect of inclination of the duct with respect to the chord line is shown in reference 4 to have a marked effect upon ram-pressure recovery. Inclination of the internal-flow system approximately  $10^\circ$  to the chord line was shown in the reference to be beneficial to the ram-pressure recovery.

Pressure and velocity distribution.— The pressure-coefficient distributions over the center of the upper surface of each design inlet are shown in figures 5, 7, 9, and 11. The pressure coefficients between the leading edge and the 15- to 20-percent-chord station were greater or less than those over the plain airfoil, depending on the inlet-velocity ratio. In general, the pressure coefficients for values of inlet-velocity ratio less than 0.4 to 0.8 were more negative than those over the plain airfoil. The critical Mach numbers of the inlets compared to the plain airfoil are shown in figures 4, 6, 8, and 10. These critical Mach numbers were estimated by the method of reference 20 from the maximum local velocities over the inlet lips and over the plain airfoil.

Comparison of the pressure distributions for the inlets with those for the plain airfoil for stations between approximately 15- to 20-percent chord and 50- to 60-percent chord revealed that, in this region, the pressure coefficients over the ducted sections were less negative than those for the plain airfoil for all test values of inlet-velocity ratio. From the 50- to 60-percent station to the trailing edge, the pressure distributions remained essentially unchanged from those of the plain airfoil.

Analysis of the pressure distributions over the design inlets revealed that a change in inlet-velocity ratio introduced an increment of velocity over the outer surface of the inlets that had a linear variation with inlet-velocity ratio. For a given inlet, the increment of local-velocity ratio corresponding to an inlet-velocity ratio of unity was evaluated as a function of chordwise location from the experimental pressure-distribution curves by the relation

$$\left(\frac{\Delta v_1}{V_0}\right)_{(V_1/V_0) = 1} = \frac{(V_2/V_0)_{(V_1/V_0) = n} - (V_2/V_0)_{(V_1/V_0) = m}}{m - n} \quad (11)$$

where  $n$  and  $m$  are two values of inlet-velocity ratio with  $m$  greater than  $n$ . Figure 15(a) presents the values of

$$\left(\frac{\Delta v_1}{V_0}\right)_{(V_1/V_0) = 1}$$

from the experimental pressure-distribution data of lip 13 (fig. 7(a)) where  $n = 0$  and the value of  $m$  is indicated in the figure. The data shown in figure 15(a) indicate that the velocity-increment ratio can be represented by a single curve. Similar curves for various upper- and lower-lip shapes and for inlet-velocity ratios from 0 to 1.6 and angles of attack from  $0^\circ$  to  $8^\circ$  are presented in figure 15(b). Analysis indicated that the increment-ratio curve was dependent on the size and location of the leading-edge radius and independent of the external shape or the angle of attack. It was noted that the effect of change in inflow rate on the velocity distribution over an inlet lip tended to vanish behind the maximum thickness. For purposes of computation, the effect was found to be negligible behind the 15- to 20-percent chord station.

The indication that the use of the velocity-increment ratio permits the calculation of the change in pressure distribution caused by variations of inlet-velocity ratio suggests a means for shortening and simplifying wind-tunnel or flight investigations of air-induction systems. Rather than record the pressure distributions corresponding to numerous inflow

rates, it would suffice to record the pressure distribution for a minimum of two inlet-velocity ratios and apply the velocity-increment-ratio principle to the calculation of the pressure distribution occurring with other inlet-velocity ratios.

Predicted drag-divergence Mach numbers.— A method of predicting the Mach number for drag divergence of airfoil sections from the low-speed pressure distributions and the airfoil profiles was developed in references 21 and 22. Briefly stated, the free-stream Mach number at which the abrupt supercritical drag rise began was shown to be that Mach number at which local sonic velocity occurred at the airfoil crest, the crest being defined as the point at which the airfoil surface is tangent to the free-stream direction. It was found that the free-stream Mach number for which sonic velocity occurred at the airfoil crest could be estimated by the Prandtl-Glauert relations. The method is believed to be directly applicable to NACA 6-series airfoils with leading-edge inlets, since reference 11 has shown experimentally that variations of section characteristics caused by compressibility for a ducted airfoil closely paralleled those for the comparable plain airfoil.

Figure 16 presents a comparison of the predicted critical and the predicted drag-divergence Mach numbers for the plain airfoil and the airfoil with inlet 3-6 (fig. 5(c)). These data indicate that the angle-of-attack range for high drag-divergence speeds would extend over at least twice the angle-of-attack range for high critical Mach numbers. In addition, the Mach number for drag divergence, being dependent on the pressures behind 10 to 15 percent of the chord, is practically independent of the inlet-velocity ratio at small angles of attack. The predicted drag-divergence Mach numbers of the design inlets tested (the data in figure 16(b) given by inlet 3-6 are representative of all the design inlets) were greater than those of the plain airfoil. This increase may possibly permit a designer to use a thicker airfoil section if combined with a leading-edge inlet.

#### Modified Inlets

Upper-lip radius.— The maximum lift characteristics of the airfoil with the design inlets were, in general, satisfactory. However, the lip pressure distributions for inlet-velocity ratios of less than unity showed the formation of a pressure minimum near the leading edge at angles of attack within the low-drag range of the plain airfoil. In an attempt to obtain a pressure gradient near the leading edge (at low values of inlet-velocity ratio) similar to that of the plain airfoil, the upper-lip radius of the inlets having ratios of the entrance height to the maximum airfoil thickness of 0.15 and 0.20 was varied from the design values of 0.00646c and 0.00575c to 0.003c and 0.002c, respectively.

The effects of changes of the lip radius on the maximum lift coefficient and on the critical Mach number of the airfoil with the inlets are shown in figure 17 for several inlet-velocity ratios. It is noted that, from consideration of maximum lift, the design radius was close to optimum. With lip radii less than that of the design, the maximum lift decreased rapidly at low inlet-velocity ratios. However, the negative pressure peaks at the leading edge of the lip at low inlet-velocity ratios were improved by decreasing the lip radius below that of the design. As shown in figure 19(a), a lip radius of 0.0045c gave a favorable pressure distribution that at zero inlet-velocity ratio was similar to that of the airfoil. With increasing inlet-velocity ratio, the pressure coefficients over the inlet became less negative than those over the airfoil, resulting in a more favorable pressure gradient. The characteristics of an inlet with an upper-lip radius of 0.0045c and a ratio of inlet entrance height to maximum airfoil thickness of 0.20 are given in figures 18(b) and 19(b).

In an attempt to reduce the inlet-velocity ratio for maximum lift with the larger inlet entrance heights, the upper-lip radius of the modified inlet shown in figures 10(b) and 11(b) was made greater than that given by the design method as indicated in table I. With the increased lip radius, the maximum lift of the airfoil with the inlet operating at an inlet-velocity ratio of approximately 0.9 was equal to that of the plain airfoil. Comparison with the results in figure 12 shows that larger values of lip radius than those indicated by equation (2) appear to be beneficial in reducing the minimum inlet-velocity ratio required to provide maximum lift with inlets having large ratios of entrance height to the maximum airfoil thickness.

External lip shape.—To study the effect of variation of the external lip shape on the pressure distribution of inlets with a ratio of entrance height to maximum airfoil thickness of 0.15 and 0.25, the inlet contour was changed as indicated in figures 20 and 21. The peak negative pressure coefficients at the leading edge became less negative for inlet-velocity ratios less than unity as the average thickness of the lip was increased. However, the pressure coefficients from approximately 5 to 25 percent of the airfoil chord became more negative. Behind the latter station, the pressure distribution was practically independent of the lip shape or the inlet-velocity ratio. The thickness of the lip cannot be increased indefinitely without causing the formation of peak negative pressure coefficients a short distance behind the leading edge.

The maximum lift and ram-pressure-recovery characteristics of the inlet with the modified lips illustrated in figures 20 and 21 remained unchanged from those of the design inlets shown in figures 4 and 8. The thinner lips of inlets 11-2 and 31-16 provided a loss of maximum lift with no internal flow, but the loss of lift was recovered for inlet-velocity ratios of 0.4 or greater. The external surfaces of the lower lip were varied in a similar manner, but, as they had a negligible effect on the pressure distribution on the upper surface and no apparent effect on the lift or ram-pressure-recovery characteristics, the results are not presented.

Comparison of the velocity distribution corresponding to the pressure distribution for any two of the upper lips of the inlets shown in figure 20 (or 21) revealed a constant systematic difference between the two velocity-distribution curves for any given value of inlet-velocity ratio. These differences are designated as velocity-increment ratios  $\Delta v_s/V_o$ . An equation, the solution of which yields the value of  $\Delta v_s/V_o$  directly, is developed in the base-profile section of the airfoil theory of reference 23. The calculation of the velocity-increment ratio  $\Delta v_s/V_o$  resulting from a change in either the upper- or lower-lip external ordinates is accomplished by a solution of the equation using a method of numerical evaluation. A sample calculation of the velocity distribution, resulting from a change in the ordinates of the upper lip 1 in figure 20 to those of lip 9, is given in the appendix and the results are shown in figure 22. A comparison of the computed velocity distributions with the experimental velocity distribution for lip 9 is presented in figure 22(c) for several values of lift coefficient and an inlet-velocity ratio of 0.4. Computations made for any inlet-velocity ratio (0 to 1.6) and lift coefficient within the linear range of lift coefficients agreed equally well with the experimental results. Similar agreement between the computed and experimental velocity distributions was obtained for lip 11 (fig. 20) with lip 1 as the reference and for lips 29 and 31 (fig. 21) with lip 23 as the reference.

#### End-Closure Shape

The final step in the design of a leading-edge inlet is the development of an end-closure shape to permit the ducted airfoil section to fair smoothly into the plain airfoil in the spanwise direction. Results from wind-tunnel programs in which leading-edge inlets were developed for specific airplanes have indicated that both semicircular and rectangular end-closure shapes are unsatisfactory. With these types of closure, the short distance in the spanwise direction between the ducted and plain airfoil sections resulted in abrupt transition sections. End-closure shapes that faired into the plain airfoil in a distance from 1.5 to 2.0 times the inlet entrance height were satisfactory. The type of end-closure shape developed in this investigation is shown in figure 23. The chordwise profile of the inlet between spanwise stations N and O was obtained from design steps 1 and 2, while the profile at stations M and P remained that of the plain airfoil. The inlet between stations M and N and between stations O and P was closed in a distance of 1.5 times the entrance height. The external transition surfaces were formed by joining the same chordwise stations on the ducted and plain airfoil sections with smooth and fair curves.

The type of closure shape indicated in figure 23 was tested on the airfoil with inlet 19-12 as shown in figure 2(a), and the results are given in figure 24. The upper-surface pressure distribution and ram-pressure recovery at the midspan of the inlet and the lift characteristics

of the airfoil with the inlet and fairing shown in figure 2(b) were previously shown in figures 18(b) and 19(b). The pressure distribution over section B (fig. 24(a)) did not show as large an effect of inlet-velocity ratio as did the distribution over the midspan station. The pressure distribution was not measured over sections C or D. As shown in figure 24(b), the ram-pressure recovery was relatively uniform along the span of the inlet. The drag and pitching-moment characteristics are shown in figure 24(c). A small change in the longitudinal stability resulted from the addition of inlet 19-12 to the airfoil, but there was no appreciable effect of inlet-velocity ratio other than that associated with the loss of maximum lift at low values of inlet-velocity ratio.

#### DESIGN INLET FOR THE NACA 4418 AIRFOIL

To check the applicability of the design method to a radically different section, a leading-edge inlet was applied to the NACA 4418 airfoil section, and two-dimensional tests of this section were made in an 8- by 36-inch wind channel. The inlet was designed by the method outlined in the section entitled "Derivation of Inlet Profile" under the heading "Design of Inlets for Cambered Profile." The ratio of the inlet entrance height to the maximum airfoil thickness was 0.21 and the lips were staggered  $10^\circ$ . Ram-pressure recovery, external drag, and maximum lift were not measured. Both the critical and drag-divergence Mach numbers were predicted from pressure-distribution data. The critical Mach numbers of the airfoil with the inlet for an inlet-velocity ratio of 0.4 were similar to those of the plain airfoil at section lift coefficients from -0.4 to 1.0. At higher inlet-velocity ratios, the predicted critical Mach numbers were above those of the plain airfoil. Also, at an inlet-velocity ratio of 0.4, the inlet operated without a pressure peak at the nose at section lift coefficients from 0.27 to 0.8. The predicted drag-divergence Mach number of the airfoil with the inlet was greater than that of the plain airfoil by approximately 0.03 for a section lift coefficient of 0.4. These data indicate that an inlet profile derived by the design method for a cambered airfoil did not reduce the estimated critical or drag-divergence Mach number of the section for inlet-velocity ratios greater than 0.4. No detrimental effects on other aerodynamic characteristics would be expected.

#### ESTIMATION OF VELOCITY DISTRIBUTION OF INLETS

No direct computational method is currently available for the prediction of the velocity distribution over an inlet in the leading edge of an airfoil. A semianalytical method is presented whereby the effects of changes in inlet ordinates and inlet-velocity ratio can be calculated.

It is stated in reference 17 that in the determination of the velocity distribution over a given airfoil, the effects of thickness distribution,

of camber, and of additional lift may be considered as separate and independent components as follows:

$$\frac{V_l}{V_o} = \frac{v}{V_o} \pm \frac{\Delta v}{V_o} \pm \frac{\Delta v_a}{V_o} \quad (12)$$

The values of the velocity-increment ratios  $\Delta v/V_o$  and  $\Delta v_a/V_o$  for most conventional and low-drag NACA airfoil sections are tabulated in reference 17.

For an airfoil having an inlet in the leading edge, the local velocity ratio is assumed to be composed of the above velocity-increment ratios with the basic velocity ratio of the airfoil  $v/V_o$  replaced by the ratio  $v_b/V_o$  for the ducted airfoil. At present, the basic velocity ratio  $v_b/V_o$  can be determined only by experiment. As mentioned previously, the effect of inlet-velocity ratio on the ducted-airfoil velocity distribution can be represented by the increment ratio  $(\Delta v_1/V_o)_{(V_1/V_o) = 1}$ . This fact permits

the calculation of the velocity distribution corresponding to any value of inlet-velocity ratio as follows:

1. Multiply the increment ratio  $(\Delta v_1/V_o)_{(V_1/V_o) = 1}$  by a constant equal to the difference between the inlet-velocity ratio for the basic velocity distribution and the given inlet-velocity ratio.
2. Add this product to the basic velocity ratio with proper regard to sign.

Changes in the velocity distribution caused by a change in the external ordinates of the lip can be evaluated by the application of thin-airfoil theory as previously discussed under the subheading External Lip Shape. Thus the local-velocity ratio of a ducted airfoil may be represented as follows:

$$\frac{V_l}{V_o} = \frac{v_b}{V_o} + \frac{\Delta v_g}{V_o} \pm \text{constant} \times \left( \frac{\Delta v_1}{V_o} \right)_{(V_1/V_o) = 1} \pm \frac{\Delta v}{V_o} \pm \frac{\Delta v_a}{V_o} \quad (13)$$

A sample calculation of the velocity distribution over a given inlet profile is presented in the appendix.

The generally satisfactory agreement shown in figure 22 (and the similar agreement between any two of the upper lips illustrated in figs. 20 and 21) between the calculated and experimental velocity distributions may be taken as experimental verification of the validity of equation (13) for the velocities over ducted airfoils. The equations may be expected to apply with accuracy sufficient for design studies to calculations for

profiles varying considerably from those involved herein. Calculations made in connection with ducted airfoils, however, should be in keeping with the limits to the application of thin-airfoil theory as discussed in reference 23.

### CONCLUSIONS

The application of the results presented in this report provides a practical means of designing inlets to fit into the leading edges of straight or slightly tapered wings with thicknesses of approximately 12-percent chord or greater. The general shape of the inlets can be derived by a method that is essentially a lofting technique. The profile coordinates as well as the spanwise end-closure shapes are considered. Inlets so derived should prove satisfactory with a minimum of testing and alteration.

The results of the present study of inlets installed in the leading edge of a wing having the NACA 63<sub>1</sub>-012 section indicated the following:

1. The airfoil with an inlet devised by the design method was found to possess satisfactory aerodynamic characteristics, as compared to the plain airfoil, with regard to lift, drag, pressure distribution, and predicted drag-divergence Mach number.
2. Introduction of stagger, increasing the inlet entrance height, or decreasing the leading-edge radius of the upper lip had a deleterious effect on the maximum lift.
3. Increasing the amount of stagger and rounding the inner surface of the lower lip improved the ram-pressure recovery at high angles of attack.
4. A change in inlet-velocity ratio introduced an increment of velocity over the outer surface of an inlet that had a linear variation with inlet-velocity ratio and was found to be independent of the angle of attack throughout the linear portion of the lift curve. Behind the position of maximum thickness of the airfoil, the variation of inlet-velocity ratio had no effect on the pressure distribution.
5. With a given inlet and the experimental velocity distribution of the given inlet as a reference, the change in the external velocity distribution caused by a small change of the external ordinates of the inlet can be calculated by an application of the principles of thin-airfoil theory. The low-speed lift, drag, pitching-moment, and ram-pressure-recovery characteristics of the wing with the modified inlet, to all practical purposes, remains unchanged from those of the wing with the given inlet.

Ames Aeronautical Laboratory,  
National Advisory Committee for Aeronautics,  
Moffett Field, Calif.

## APPENDIX

SAMPLE CALCULATION OF THE VELOCITY DISTRIBUTION  
OVER A GIVEN INLET PROFILE

In order to facilitate an understanding of a procedure to be followed in estimating the velocity distribution over a given inlet when the velocity distribution of a base or reference inlet is known, an illustrative example is presented. The example chosen is that of determining the velocity distribution over lip 9 (fig. 20) for an inlet-velocity ratio of 0.4 using the coordinates and data of design lip 1 as a reference.

The increment of local-velocity ratio  $\Delta v_s/V_0$  resulting from a change in ordinate between the lip radius and the position of maximum thickness is calculated from an equation developed in thin-airfoil theory. It is shown in reference 23 that, if  $\Delta y/c$  is the difference between the ordinates of a given and a reference profile, the increment  $\Delta v_s/V_0$  due to the ordinate change can be expressed by the integral relation (equation (45) of reference 23).

$$\frac{\Delta v_s}{V_0} = -\frac{1}{2\pi} \int_0^{2\pi} \frac{d(\Delta y)}{dx} \cot \frac{(\theta - \theta_0)}{2} d\theta \quad (A1)$$

where  $\theta$  and  $\theta_0$  are new airfoil coordinates for  $x$  and  $x_0$  defined as

$$\left. \begin{aligned} x &= \frac{c}{2} (1 - \cos \theta) \\ x_0 &= \frac{c}{2} (1 - \cos \theta_0) \end{aligned} \right\} \quad (A2)$$

and the subscript  $o$  indicates the position on the  $x$  axis for which the velocity increment  $\Delta v_s/V_0$  is desired. Thus  $\theta$  and  $\theta_0$  vary from 0 to  $\pi$  along the chord of the airfoil. Use of the integral in equation (A1) presupposes the existence of a similar ordinate change on the lower surface. However, in this application the ordinate change to the lower surface is considered solely for purposes of computation, as the experimental results have shown that a modification on the lower surface has no discernible effects on the velocity distribution over the upper surface of the inlet.

The procedure is as follows: The coordinates of design lip 1, which were derived by the design method, and of lip 9, which were derived by alteration of the contour of design lip 1, are tabulated in table II. The differences between the ordinates of the given inlet and the reference inlet  $\Delta y/c$  are tabulated in table II and plotted as a

function of the chordwise position in figure 22(a). The derivative  $d(\Delta y/c)/d(x/c)$  was evaluated graphically. The values are tabulated in table II and plotted as a function of the chordwise position in figure 22(b). This derivative at the leading edge and at the position of maximum thickness was arbitrarily set equal to zero.

The integral in equation (A1) can be evaluated by a numerical method as explained in reference 23. However, reference 24 presents another method of evaluation that is more easily applied and will be used in the remainder of this example. A 40-point solution of equation (A1) is

$$\begin{aligned} \frac{\Delta v_B}{V_0} = & a_{k_1} \left\{ \left[ \frac{d(\Delta y)}{dx} \right]_{-1} - \left[ \frac{d(\Delta y)}{dx} \right]_1 \right\} + \\ & a_{k_2} \left\{ \left[ \frac{d(\Delta y)}{dx} \right]_{-2} - \left[ \frac{d(\Delta y)}{dx} \right]_2 \right\} \\ & \vdots \\ & \vdots \\ & \vdots + \\ & a_{k_{20}} \left\{ \left[ \frac{d(\Delta y)}{dx} \right]_{-20} - \left[ \frac{d(\Delta y)}{dx} \right]_{20} \right\} \end{aligned} \quad (A3)$$

where

$$\left[ \frac{d(\Delta y)}{dx} \right]_1 \text{ is the value of } \frac{d(\Delta y)}{dx} \text{ at } \theta_0 + \frac{\pi}{20}$$

$$\left[ \frac{d(\Delta y)}{dx} \right]_n \text{ is the value of } \frac{d(\Delta y)}{dx} \text{ at } \theta_0 + \frac{n\pi}{20}$$

$$(n = 1, -1, 2, -2, \dots, 20, -20)$$

The value of the ordinate and the derivative at station  $\pi + \theta$  must be taken as the values at  $\pi - \theta$  but with opposite sign. Thus,

$$\left[ \frac{d(\Delta y)}{dx} \right]_{\pi+\theta} = - \left[ \frac{d(\Delta y)}{dx} \right]_{\pi-\theta}$$

Values of the computational coefficients  $a_k$ , obtained from reference 24, are tabulated in table III for the 40-point and also an 80-point solution.

In the sixth column of table II, values of chordwise station  $x/c$  corresponding to equal intervals of  $\theta$  ( $\pi/20$  for a 40-point solution and  $2\pi/40$  for an 80-point solution) are presented for the range of integration. The values of  $d(\Delta y)/dx$  for these various values of  $\theta$  were obtained from figure 22(b). Since no change of ordinate is made behind 0.35 chord, the values of  $d(\Delta y)/dx$  from  $x/c = 0.35$  to the trailing edge are equal to zero.

The value of  $\Delta v_s/V_0$  was calculated from equation (A3) as follows: Three paper tapes were arranged side by side. The first tape carried the values of  $a_k$  at appropriate intervals; the second carried the values of  $[d(\Delta y)/dx]_{-1, -2, \dots, -20}$ ; and the third, the values of  $[d(\Delta y)/dx]_{1, 2, \dots, 20}$ . By moving the latter two tapes with respect to the first, the values in the brackets of equation (A3) are brought into juxtaposition with the computational coefficients for the various values of  $\theta$ . Arranged in cyclic form, the value of  $\Delta v_s/V_0$  for  $\theta = \pi/20$  is, for example:

$$\begin{aligned} \Delta v_s/V_0 = & [ 0.5287 \quad (0 - 0.0600) + \\ & 0.14824 \quad (-0.0680 - 0.0136) + \\ & 0.07614 \quad (-0.0600 + 0.0041) + \\ & 0.10259 \quad (-0.0136 + 0.0115) + \\ & 0.04024 \quad (0.0041 + 0.0144) + \\ & 0.06542 \quad (0.0115 + 0.0096) + \\ & 0.02720 \quad (0.0144 + 0.0006) + \\ & 0.04588 \quad (0.0096 + 0) + \\ & 0.01951 \quad (0.0006 + 0) + \\ & 0.03333 \quad (0 + 0) + \dots ] = -0.045 \end{aligned}$$

The values of  $\Delta v_s/V_0$  for  $0 < \theta \leq 8\pi/20$  are given in table II. For purposes of comparison, the values of  $\Delta v_s/V_0$  for  $0 < \theta \leq 10\pi/40$  were computed using the 80-point solution and are also given in table II. It is readily apparent that near the leading edge a large difference existed in the calculated value of  $\Delta v_s/V_0$ , depending on the type of solution. On the basis of comparison with experimental results, the values obtained by use of the 80-point solution were satisfactory. Values obtained by use of a 160-point solution were in slightly closer agreement with the experimental results. However, the difference between the

values obtained by the 160-point solution compared to the 80-point solution did not warrant the additional calculations. It is recommended that, in determining the value of  $\Delta v_s/v_o$ , the 80-point solution be used in the interval  $0 < \theta \leq 8\pi/40$  and that the 40-point solution be used for the remainder of the interval up to the location of maximum thickness.

For an inlet-velocity ratio of 0.4 and at an angle of attack of  $0^\circ$  (zero lift), the velocity distribution over lip 1 was determined experimentally (fig. 4) and is tabulated in table II. The velocity distribution over lip 9 was found from

$$\left( \frac{v_l}{v_o} \right)_{\text{lip 9}} = \left( \frac{v_b}{v_o} \right)_{\text{lip 1}} + \frac{\Delta v_s}{v_o} \pm C_L \left( \frac{\Delta v_a}{v_o} \right) \quad (A4)$$

$C_L = 1$

The value of  $\Delta v_a/v_o$  was assumed equal to that of the NACA 63<sub>1</sub>-012 airfoil. The computed velocity distribution over lip 9 is tabulated in table II and is shown in the insert of figure 22(c). The distribution for various values of lift coefficient is shown in figure 22(c) compared to the experimental velocity distribution.

The low-speed pressure coefficients are calculated from the velocity distribution by the relation.

$$P = 1 - \left( \frac{v_l}{v_o} \right)^2 \quad (A5)$$

The variation of pressure coefficient with Mach number can be estimated by the Karman-Tsien compressibility relations, as discussed in reference 25.

#### REFERENCES

1. Biermann, David, and Corson, Blake W., Jr.: Model Tests of a Wing-Duct System for Auxiliary Air Supply. NACA ACR, Jan. 1941.
2. Bartlett, Walter A., Jr., and Goral, Edwin B.: Wind-Tunnel Investigation of Wing Inlets for a Four-Engine Airplane. NACA RM L6L11, 1947.
3. Harmon, Hubert N.: Wind-Tunnel Tests of Several Duct Entrances in the Leading Edge of an NACA 23018 Wing. NACA ARR, Oct. 1942.
4. Nelson, W. J., and Czarnecki, K. R.: Wind-Tunnel Investigation of Wing Ducts on a Single-Engine Pursuit Airplane. NACA ARR 3J13, 1943.

5. Biermann, David, and McLellan Charles H.: Wind-Tunnel Investigation of Rectangular Air-Duct Entrances in the Leading Edge of an NACA 23018 Wing. NACA ACR, Sept. 1940.
6. Spence, A., and Seddon, J.: A Review of Wing Leading Edge Entry Design, Based on the Results of Model Tests at the R. A. E. Rep. No. Aero 1989, R. A. E. (British), Nov. 1944.
7. Racisz, Stanley F.: Development of Wing Inlets. NACA ACR L6B18, 1946.
8. Scherer, A.: Investigations on Nose Inlets of Rectangular Wings. M. A. P. Volkenrode Ref: MAP - VG 166-T, July 15, 1947.
9. Ruden, P.: Wind Tunnel Measurements on Flat Symmetrical Scoop Diffusers. FB 1325, ZWB (Berlin), 1940.
10. von Doenhoff, Albert E., and Horton, Elmer A.: Preliminary Investigation in the NACA Low-Turbulence Tunnel of Low-Drag Airfoil Sections Suitable for Admitting Air at the Leading Edge. NACA ACR, July 1942.
11. Smith, Norman F.: High-Speed Investigation of Low-Drag Wing Inlets. NACA ACR L4I28, 1944.
12. Kuchemann, D., and Weber, J.:  $J_2$  Power Unit Ducts.- 6.5 Experimental Investigations on Flat Double-Profiles. British, M. A. P. Volkenrode AVA Monographs, Rep. and Trans. 990, July 15, 1948, pp. 40 - 83.
13. Perl, W., and Moses, H. E.: Velocity Distributions on Two-Dimensional Wing-Duct Inlets by Conformal Mapping. NACA TR 893, 1948.
14. Temple, G., and Yarwood, Jennifer: Two-Dimensional Aerofoils and Ducts with Uniform Velocity Distribution. R. & M.No. 2090, British A. R. C., 1944.
15. Ruden, P.: Two-Dimensional Symmetrical Inlets With External Compression. NACA TM 1279, 1950.
16. Brodel, Walter: Theory of Plane Symmetrical Intake Diffusers. NACA TM 1267, 1950.
17. Abbott, Ira H., von Doenhoff, Albert E., and Stivers, Louis S., Jr.: Summary of Airfoil Data. NACA Rep. 824, 1945.
18. Allen, H. Julian, and Vincenti, Walter G.: Wall Interference in a Two-Dimensional-Flow Wind Tunnel, With Consideration of the Effect of Compressibility. NACA Rep. 782, 1944.
19. Becker, John V.: Wind-Tunnel Tests of Air Inlet and Outlet Openings on a Streamline Body. NACA ACR, Nov. 1940.

20. von Kármán, Th.: Compressibility Effects in Aerodynamics. Jour. Aero. Sci., vol. 8, no. 9, July 1941, pp. 337 - 356.
21. Nitzberg, Gerald E., and Crandall, Stewart: A Study of Flow Changes Associated With Airfoil Section Drag Rise at Supercritical Speeds. NACA TN 1813, 1949.
22. Nitzberg, Gerald E., Crandall, Stewart M. and Polentz, Perry P.: A Preliminary Investigation of the Usefulness of Camber in Obtaining Favorable Airfoil-Section Drag Characteristics at Supercritical Speeds. NACA RM A9G20, 1949.
23. Allen, H. Julian: General Theory of Airfoil Sections Having Arbitrary Shape or Pressure Distribution. NACA Rep. 833, 1945.
24. Naiman, Irven: Numerical Evaluation of the  $\epsilon$  - Integral Occurring in the Theodorsen Arbitrary Potential Theory. NACA ARR L4D27a, 1944.
25. Liepmann, H. W., and Puckett, A. E.: Introduction to Aerodynamics of a Compressible Fluid. John Wiley and Sons, Inc., New York, 1947, pp. 244 - 247.

TABLE I

LEADING-EDGE INLET LIP DETAILS  
 [Dimensions are in percent of airfoil chord]

Upper lip					
d/t	Number	Radius	A	External shape	Type
0.15	1	0.646	1.37	Design step 1	Design
	3	.646	1.00	Design step 2	Do.
	5	.550	.98	Eq.(7) - Design step 2	Modified
	7	.450	.96	Eq.(7) - Design step 2	Do.
	9	.646	1.37	Faired curve	Do.
	11	.646	1.37	Faired curve	Do.
.20	13	.575	1.64	Design step 1	Design
	15	.575	1.25	Design step 2	Do.
	17	.450	1.52	Eq.(7) - Design step 1	Modified
	19	.450	1.19	Eq.(7) - Design step 2	Do.
	21	.200	1.52	Eq.(7) - Design step 1	Do.
.25	23	.510	1.90	Design step 1	Design
	25	.510	1.51	Design step 2	Do.
	27	.510	1.21	Design step 2	Do.
	29	.510	1.90	Faired curve	Modified
	31	.510	1.90	Faired curve	Do.
.30	33	.442	1.84	Design step 2	Design
	35	.543	1.46	Eq.(7) - Design step 2	Modified



TABLE I.- CONCLUDED

Lower lip					
d/t	Number	Stagger angle (deg)	Radius	B	External shape
0.15	2	0	0.300	1.37	Design step 1
	4	20	.300	1.37	Design step 1
	6	20	.300	1.58	Design step 2
	8	20	.300	1.88	Design step 2
.20	10	0	.300	1.64	Design step 1
	12	20	.300	1.82	Design step 2
	14	40	.300	1.64	Design step 1
.25	16	0	.300	1.90	Design step 1
	18	20	.300	2.09	Design step 2
	20	40	.300	2.30	Design step 2
.30	22	20	.300	2.17	Design step 1
	24	40	.300	2.58	Design step 2



TABLE II  
CALCULATION OF VELOCITY DISTRIBUTION  $V_1/V_0$

1	2	3	4	5	6	7	8	9	10	11
$\frac{x}{c}$	Ordinates, $y/c$		$\frac{\Delta y}{c}$	$\theta$ (radi- ans)	$\frac{x}{c}$	$\frac{d(\Delta y)}{dx}$	$\frac{\Delta v_s}{V_0}$		$\left(\frac{V_1}{V_0}\right)_{lip 1}$	$\left(\frac{V_1}{V_0}\right)_{lip 9}$
	Lip 1	Lip 9					40 point	80 point		
0	0.0137	0.0137	0	0	0	0	-	-	-	-
.005	.0213	.0212	-.0001	$1\pi/40$	.0015	-.0455	-	-0.066	1.001	0.935
.0075	.0229	.0230	.0001	$2\pi/40$	.0062	.0680	-0.045	-.100	1.109	1.009
.0125	.0254	.0260	.0006	$3\pi/40$	.0138	.0875	-	-.022	1.118	1.096
.025	.0299	.0314	.0015	$4\pi/40$	.0244	.0600	.022	.026	1.121	1.147
.05	.0363	.0386	.0023	$5\pi/40$	.0381	.0294	-	.029	1.126	1.151
.075	.0410	.0435	.0025	$6\pi/40$	.0545	.0136	.039	.034	1.127	1.151
.10	.0449	.0474	.0025	$7\pi/40$	.0737	.0034	-	.024	1.129	1.153
.15	.0507	.0527	.0020	$8\pi/40$	.0955	-.0041	.024	.021	1.132	1.152
.20	.0549	.0562	.0013	$9\pi/40$	.1198	-.0086	-	.016	1.135	1.151
.25	.0578	.0585	.0007	$10\pi/40$	.1465	-.0115	.015	.014	1.136	1.150
.30	.0594	.0596	.0002	$11\pi/40$	.1753	-.0144	-	-	-	-
.35	.0600	.0600	0	$12\pi/40$	.2061	-.0144	.001	-	1.149	1.150
				$13\pi/40$	.2388	-.0125	-	-	-	-
				$14\pi/40$	.2730	-.0096	-.005	-	1.151	1.146
				$15\pi/40$	.3087	-.0058	-	-	-	-
				$16\pi/40$	.3455	-.0006	-.005	-	1.152	1.147
				$17\pi/40$	.3833	0	-	-	-	-



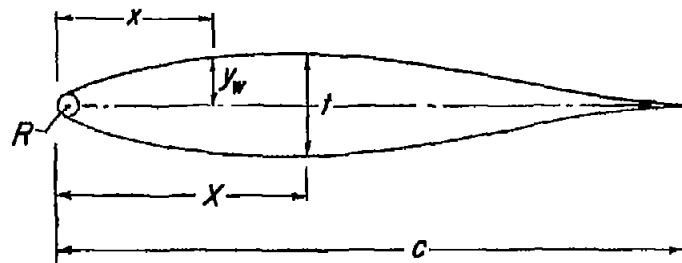
TABLE III

VALUES OF  $a_k$  FOR USE WITH EQUATION (A3)

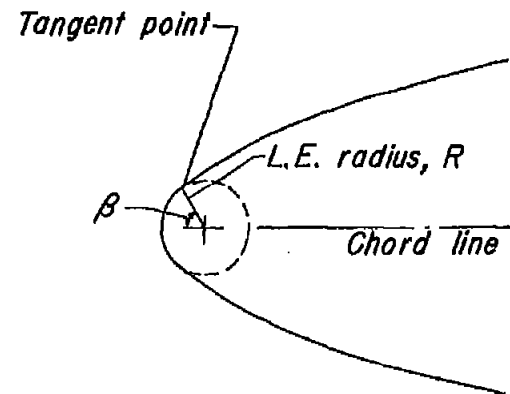
40-point method			
k	$a_k$	k	$a_k$
1	0.52827	11	0.01423
2	.14824	12	.02422
3	.07614	13	.01021
4	.10259	14	.01698
5	.04024	15	.00690
6	.06542	16	.01083
7	.02720	17	.00400
8	.04588	18	.00528
9	.01951	19	.00066
10	.03333	20	0
80-point method			
1	0.52862	21	.000770
2	.14952	22	.01423
3	.07712	23	.00656
4	.10522	24	.01210
5	.04189	25	.00556
6	.06942	26	.01021
7	.02954	27	.00466
8	.05129	28	.00849
9	.02258	29	.00384
10	.04023	30	.00690
11	.01807	31	.00307
12	.03271	32	.00541
13	.01488	33	.00235
14	.02719	34	.00400
15	.01247	35	.00165
16	.02294	36	.00264
17	.01057	37	.00098
18	.01951	38	.00131
19	.00901	39	.00032
20	.01666	40	0



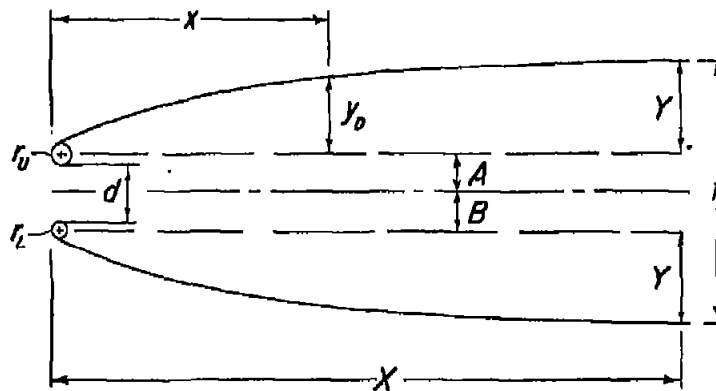




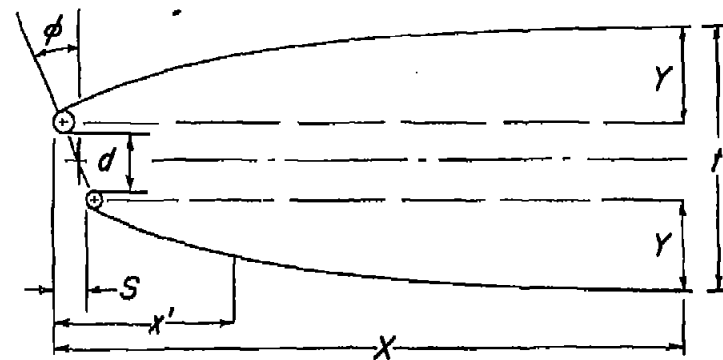
**(a) Symmetrical airfoil section.**



(c) Angle  $\beta$  as measured on symmetrical airfoil.



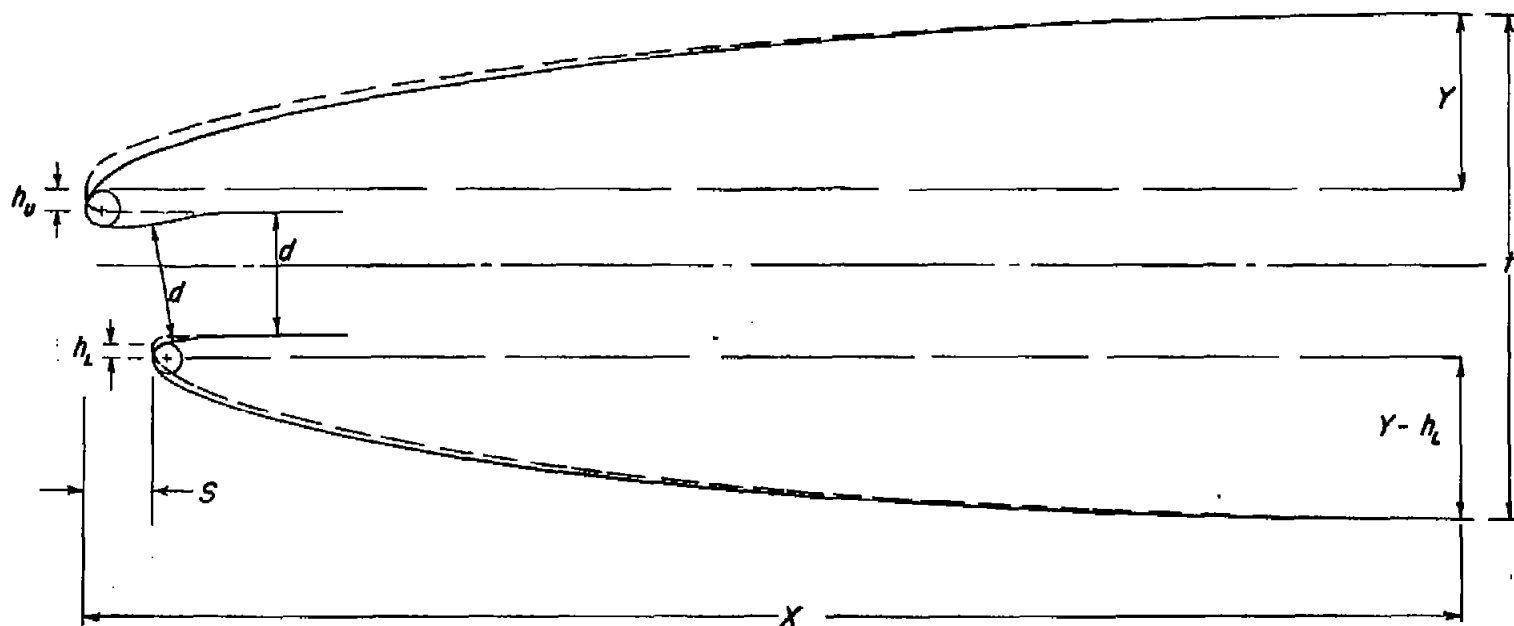
*(b) Unstaggered inlet. Design step 1.*



(d) Staggered inlet. Design step 1.



*Figure 1.- Geometric symbols used in derivation of inlet-profile coordinates.*



(e) Staggered inlet with drooped upper lip and rounded lower lip. Design step 2.



Figure 1.- Concluded.



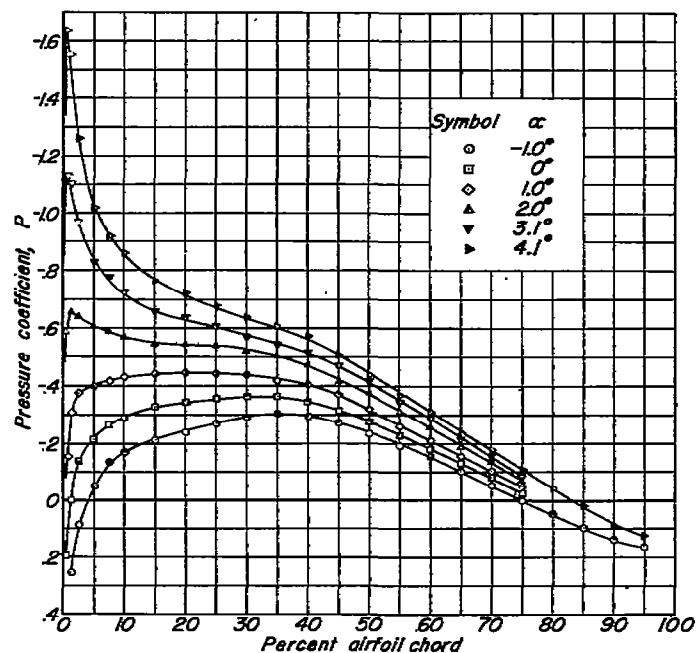
(a) Inlet with end closure shape.



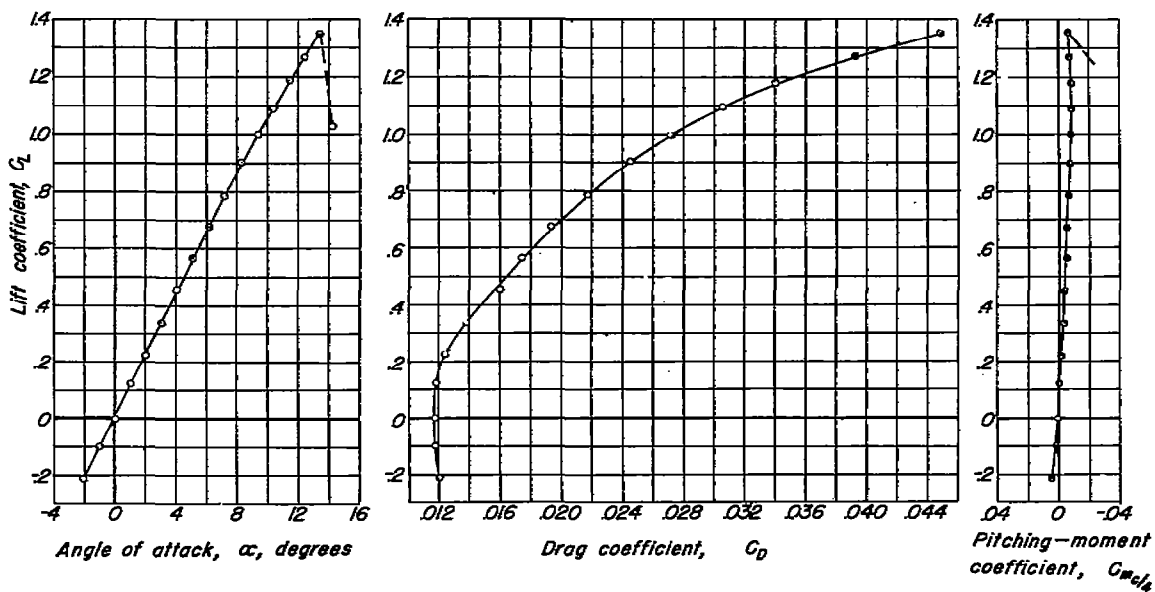
(b) Inlet with fairing.

Figure 2.- Model installation in wind tunnel.





(a) Pressure-coefficient distribution.



(b) Lift, drag and pitching-moment characteristics.



Figure 3.—Aerodynamic characteristics of the NACA 63-012 airfoil without inlets.

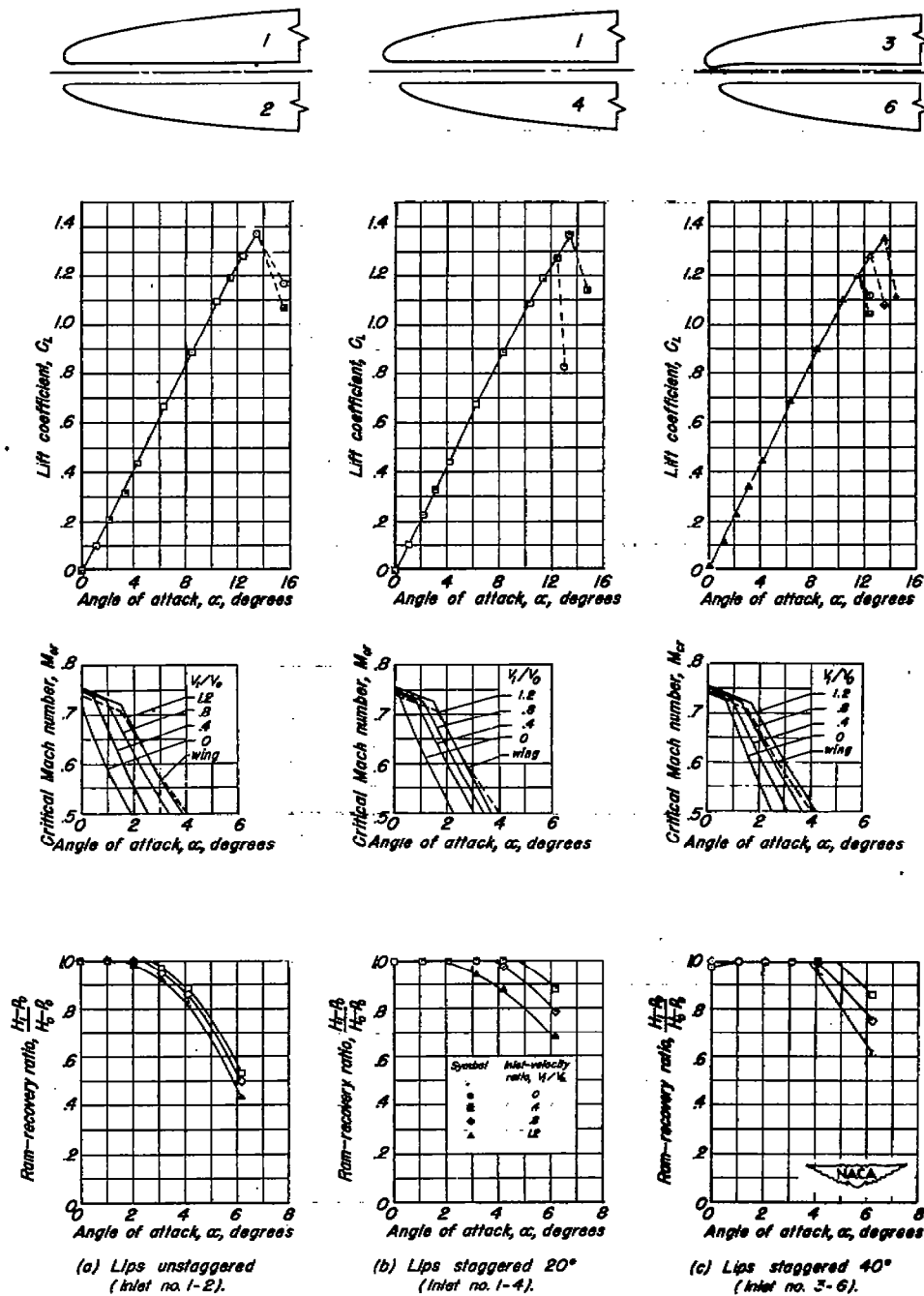


Figure 4.—General characteristics of the NACA 63-012 airfoil with design leading-edge inlets.  $d/t$ , 0.15.

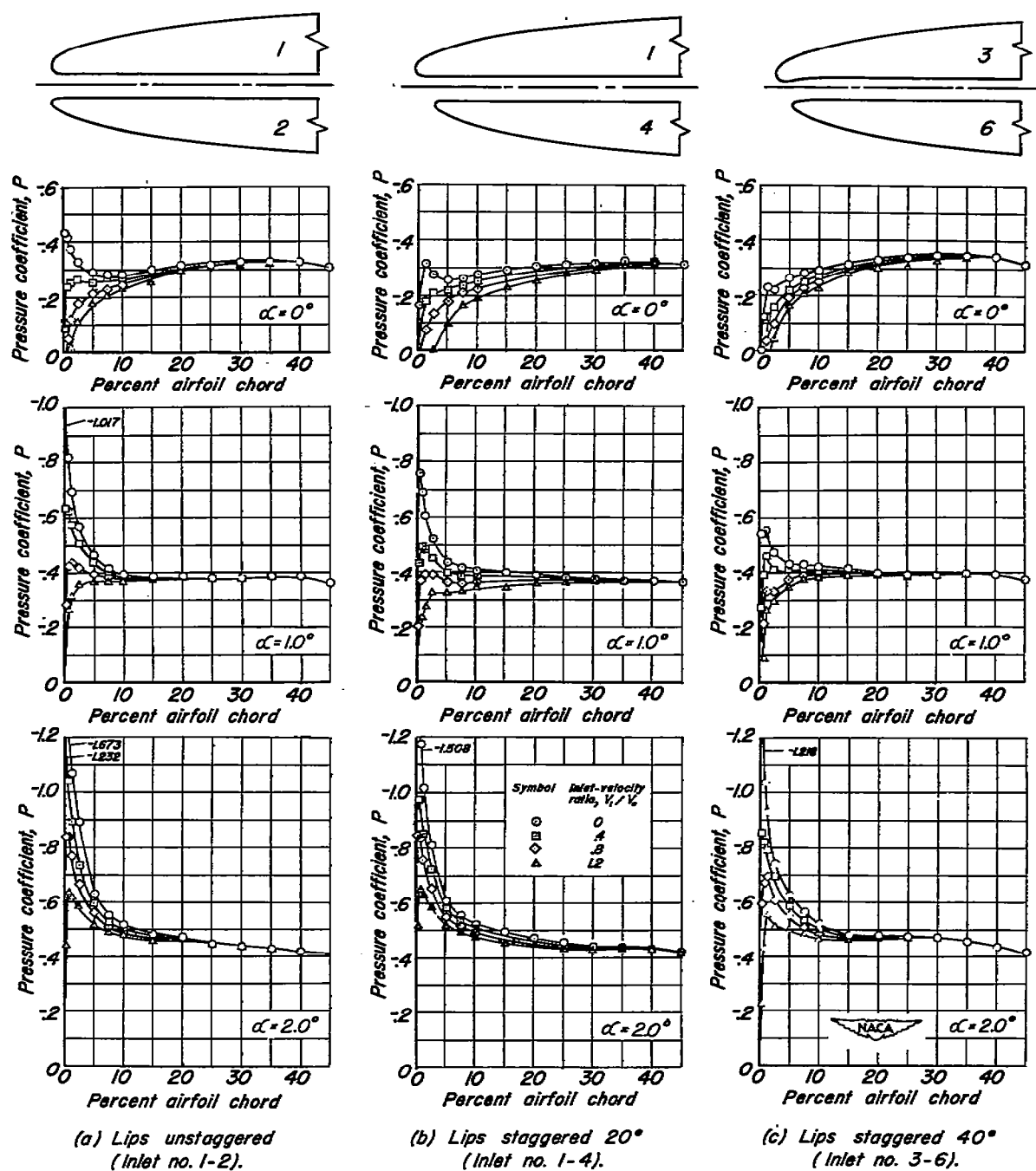


Figure 5.—External pressure distribution over the center of the upper surface of design inlets.  $d/t$ , 0.15.

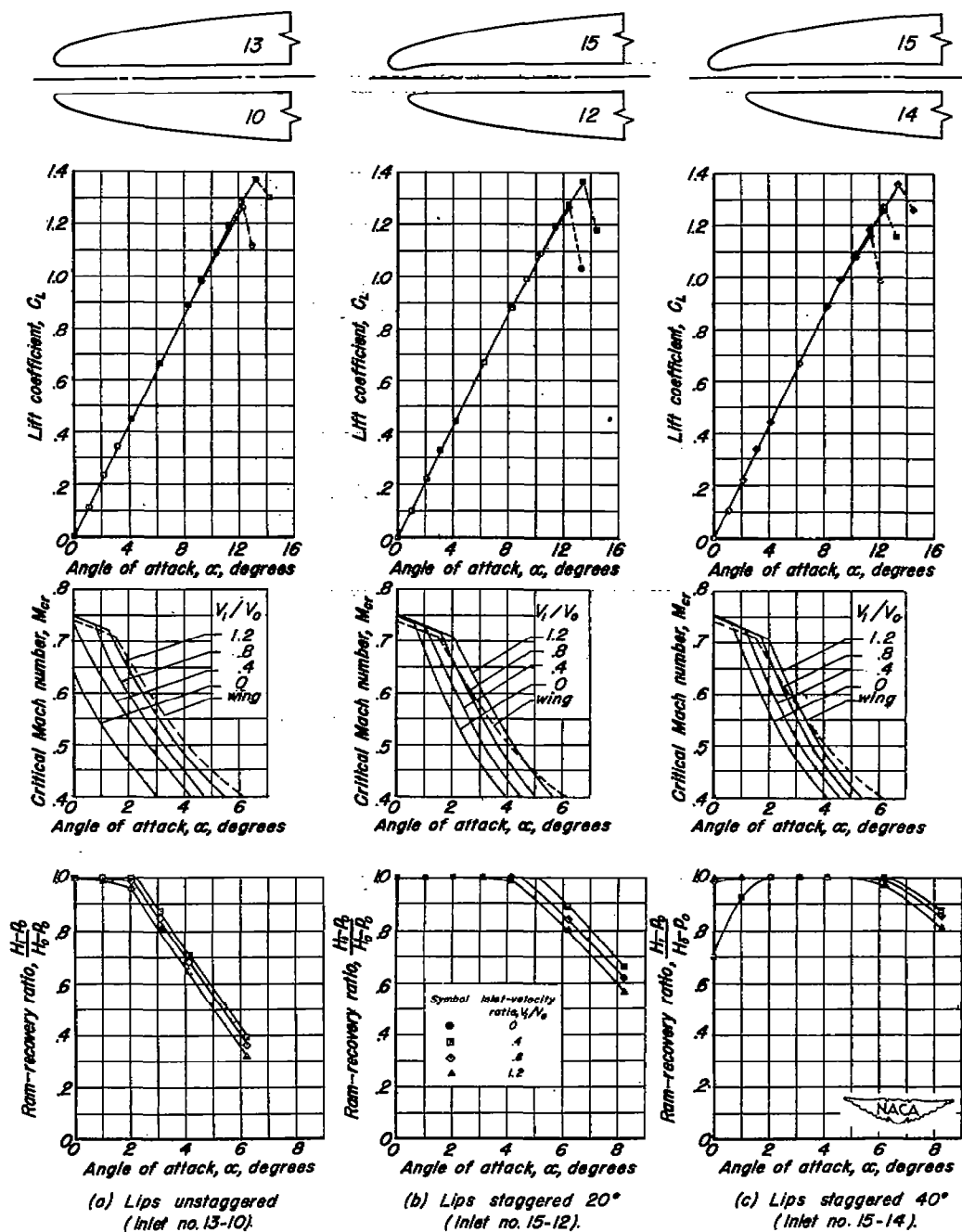


Figure 6.— General characteristics of the NACA 63-012 airfoil with design leading-edge inlets.  $d/t$ , 0.20.

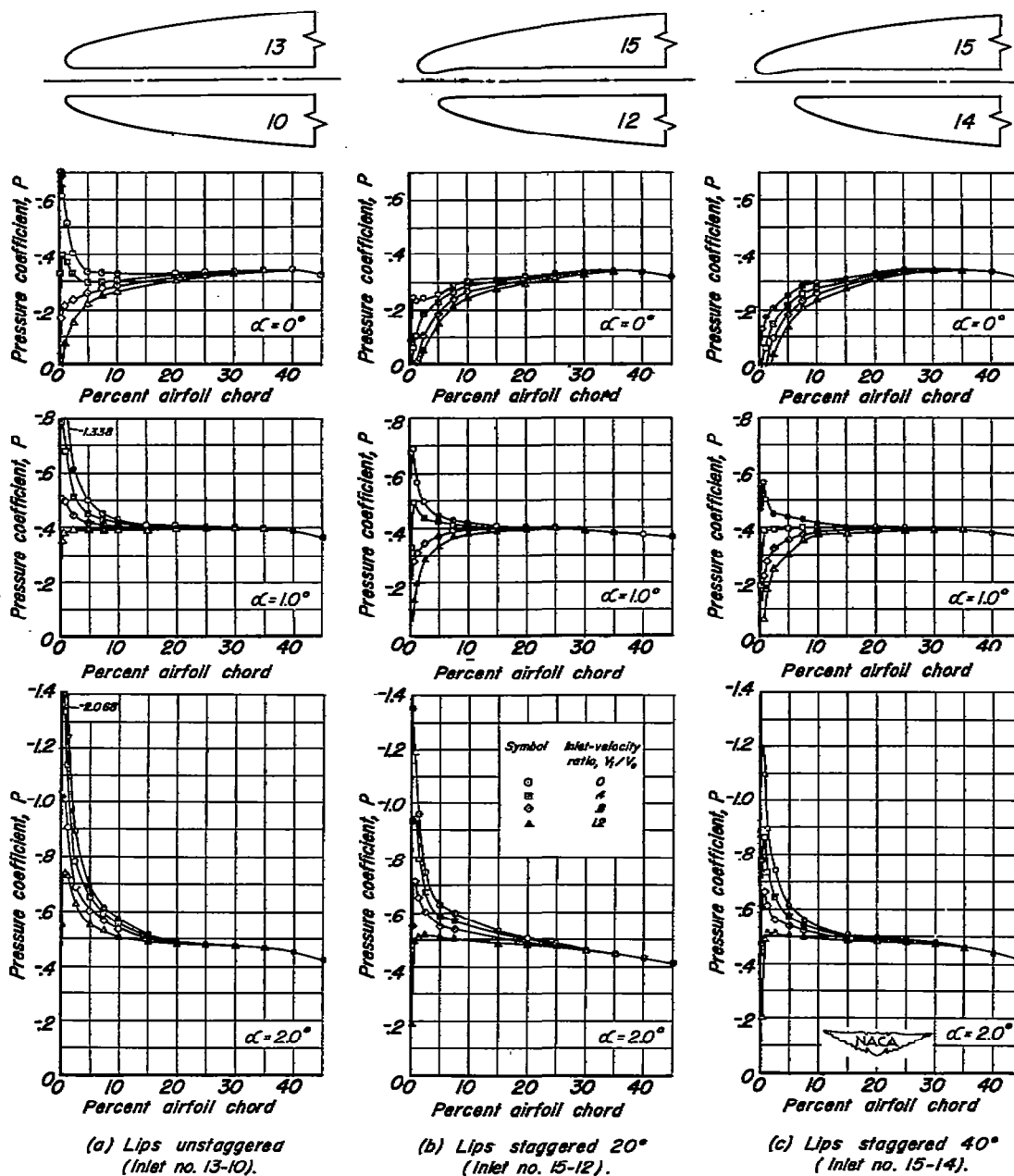


Figure 7.— External pressure distribution over the center of the upper surface of design inlets.  $d/t$ , 0.20.

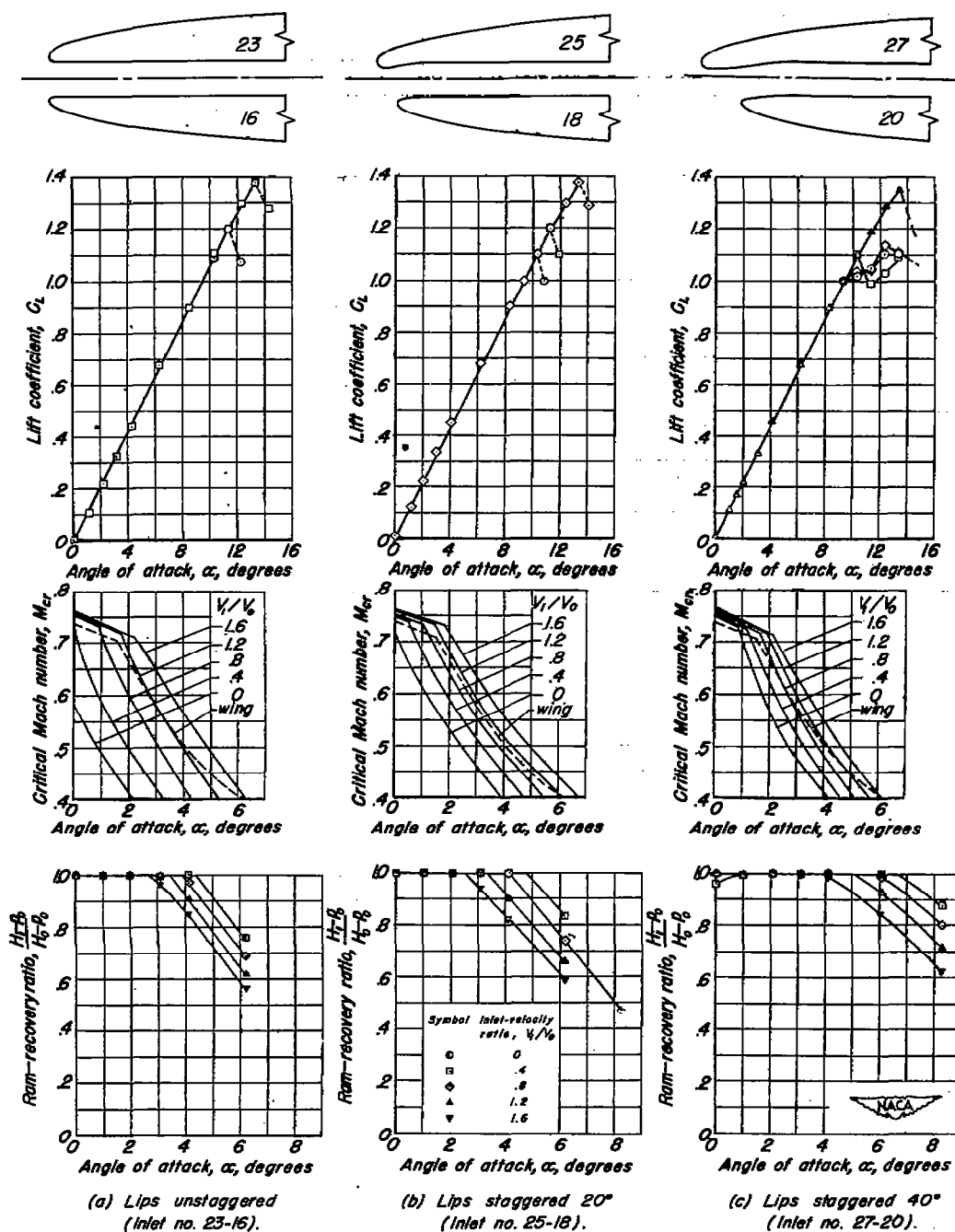


Figure 8.- General characteristics of the NACA 63-012 airfoil with design leading-edge inlets.  $d/t$ , 0.25.

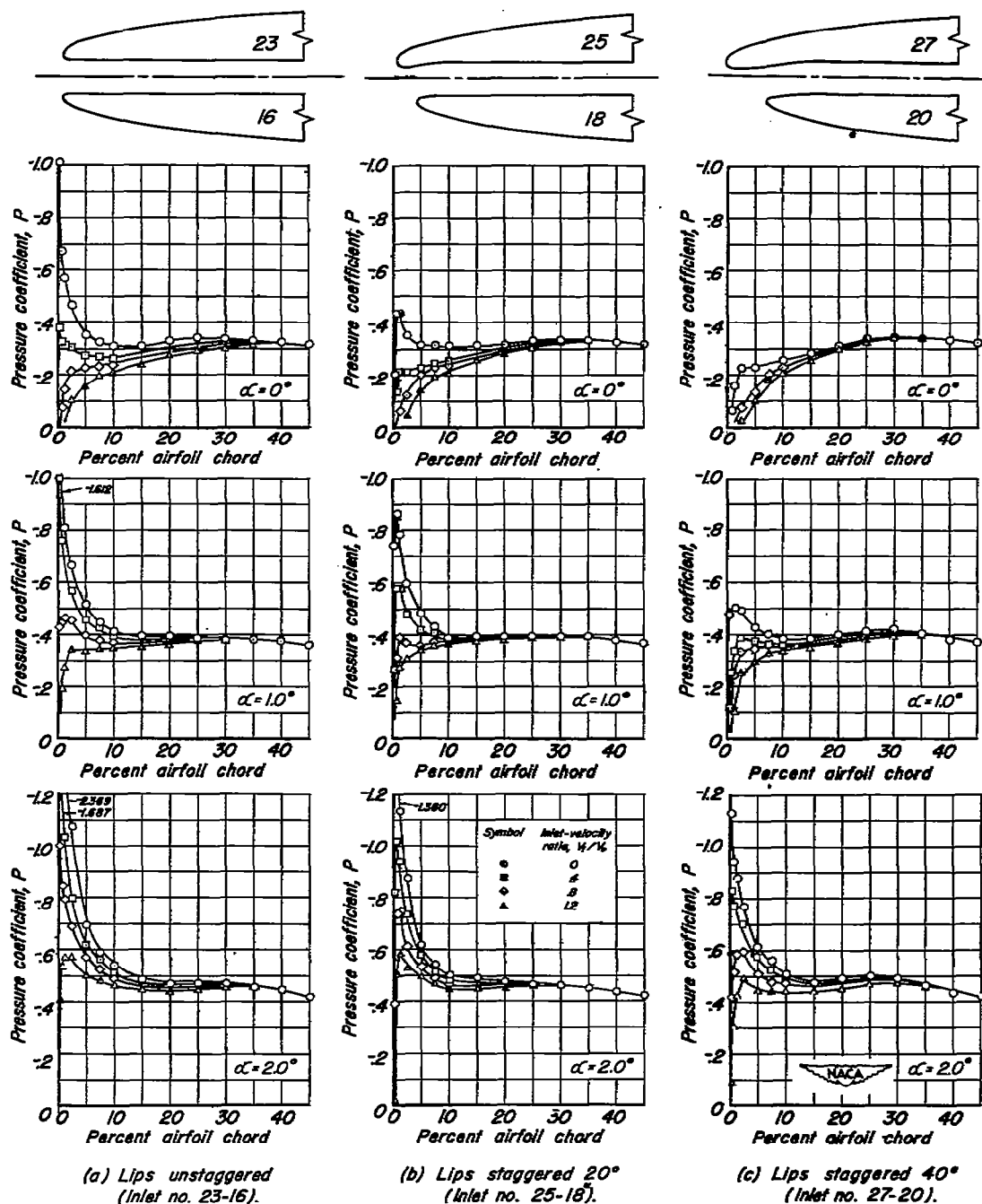


Figure 9.— External pressure distribution over the center of the upper surface of design inlets.  $d/t$ , 0.25.

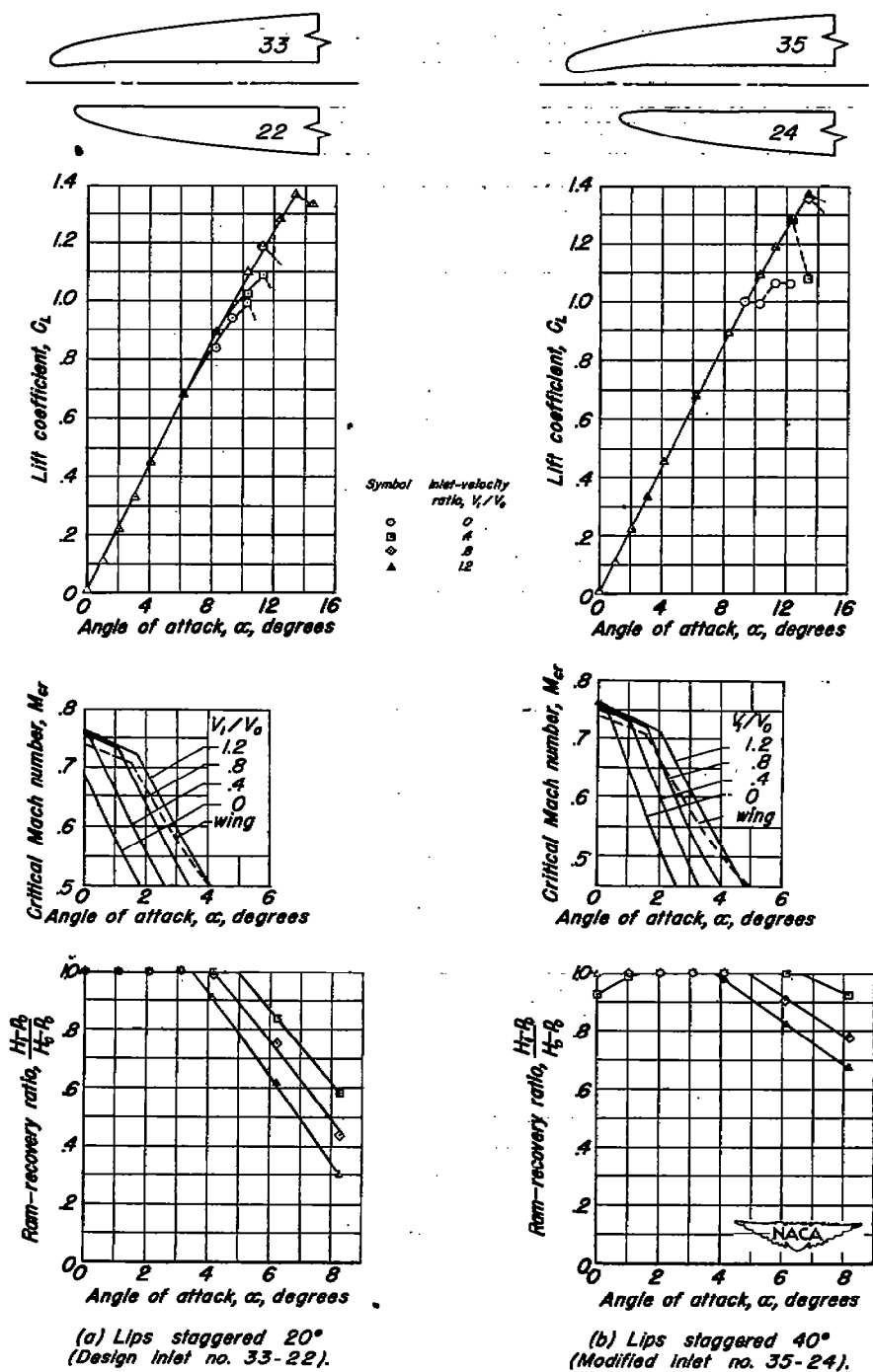


Figure 10.— General characteristics of the NACA 63-012 airfoil with a design and a modified leading-edge inlet.  $d/t$ , 0.30.

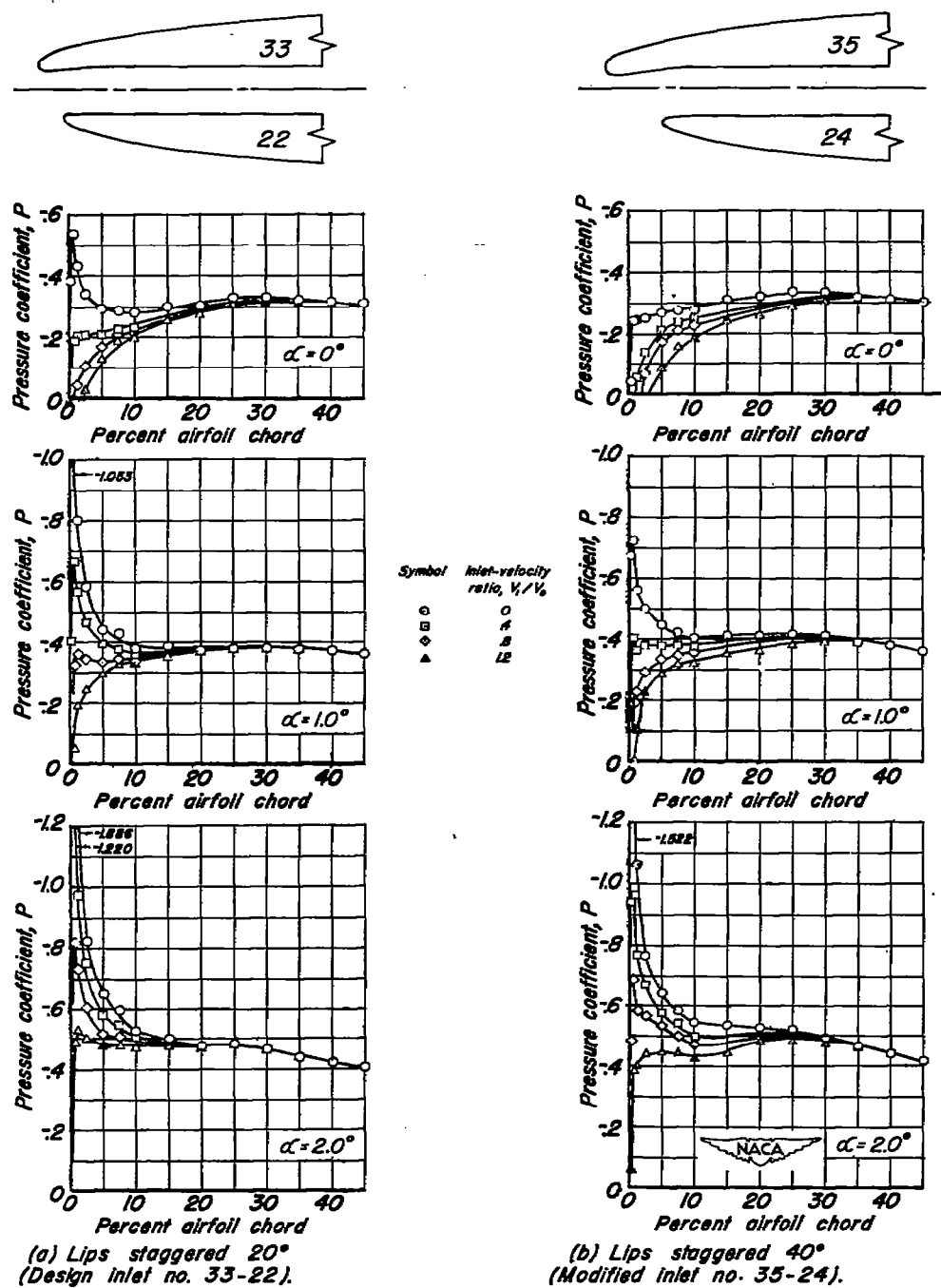


Figure 11.- External pressure distribution over the center of the upper surface of a design and a modified inlet.  $d/t$ , 0.30.

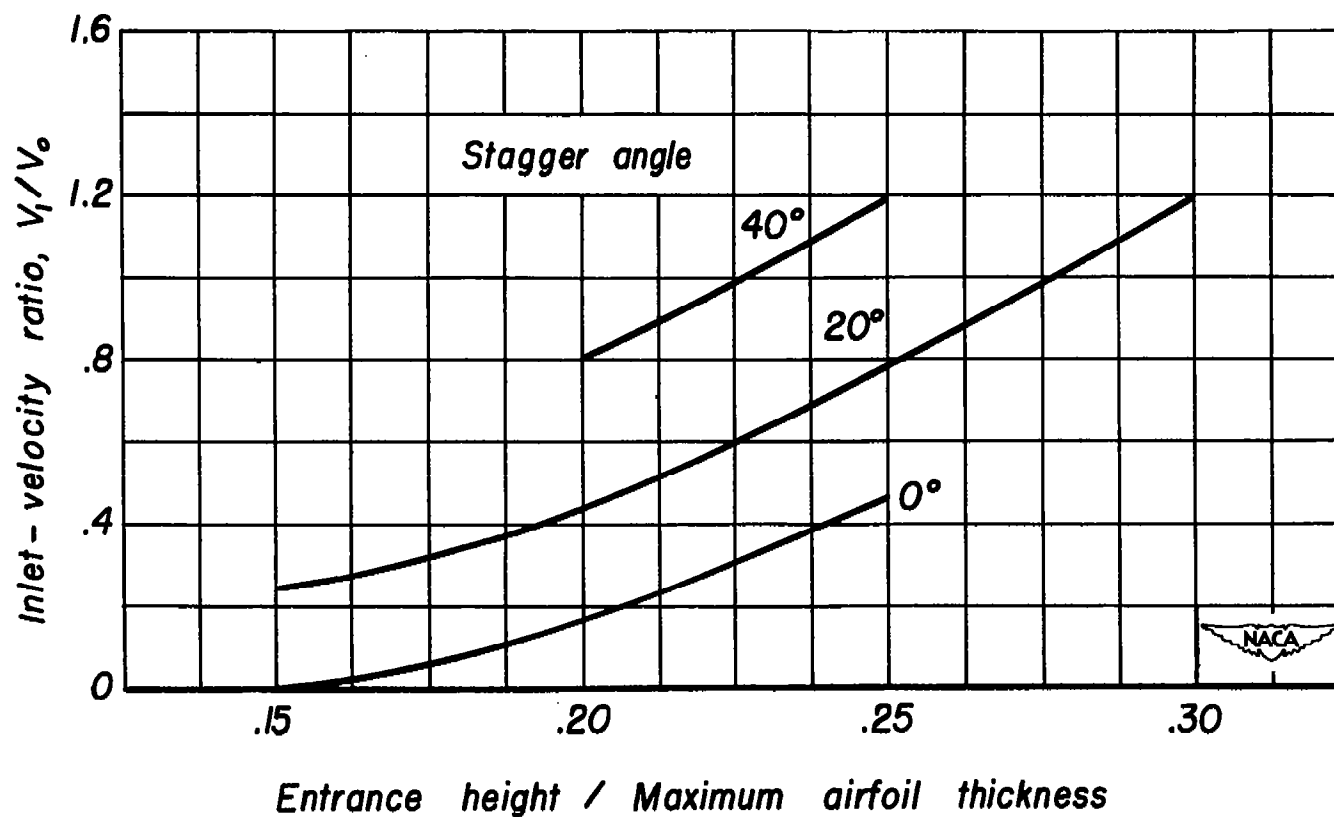


Figure 12.- Minimum inlet-velocity ratio for which the maximum lift coefficient of the airfoil with a design inlet was equal to that of the plain airfoil.

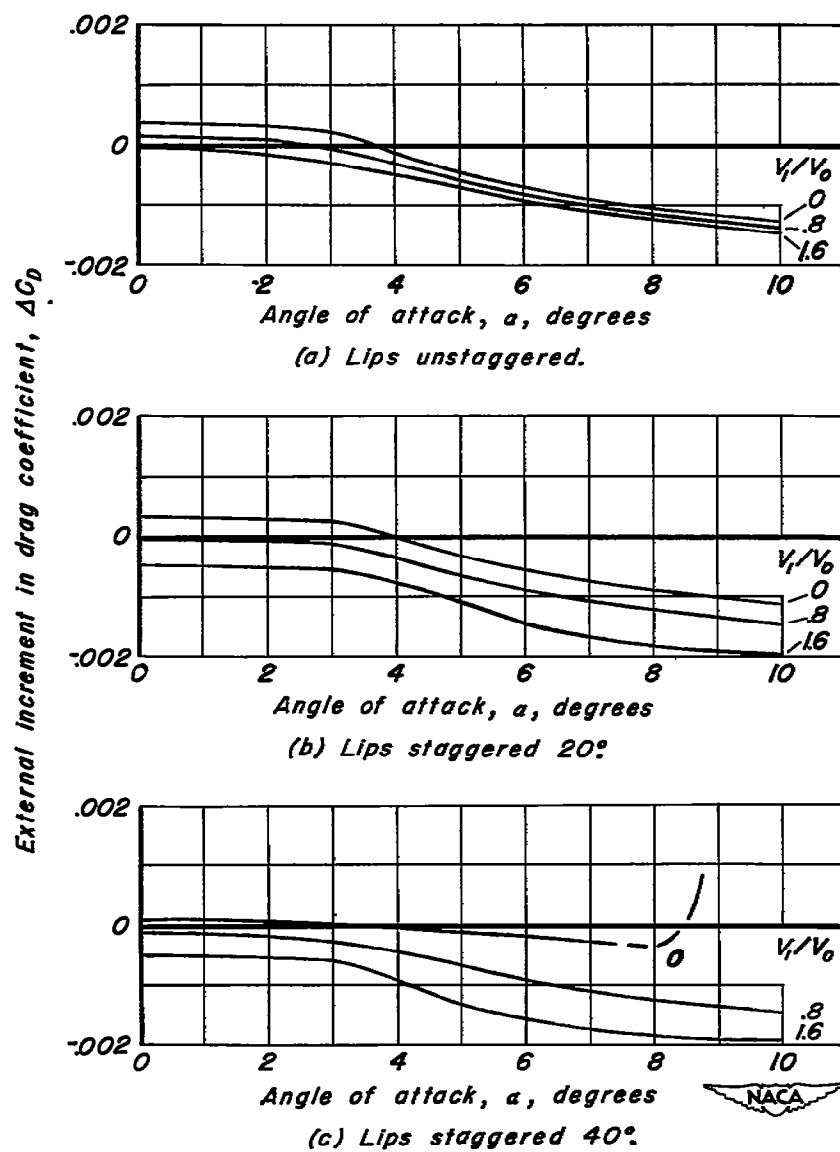


Figure 13.- Variation of the increment of external drag coefficient with angle of attack caused by the addition of design inlets on the NACA 63,-012 airfoil.

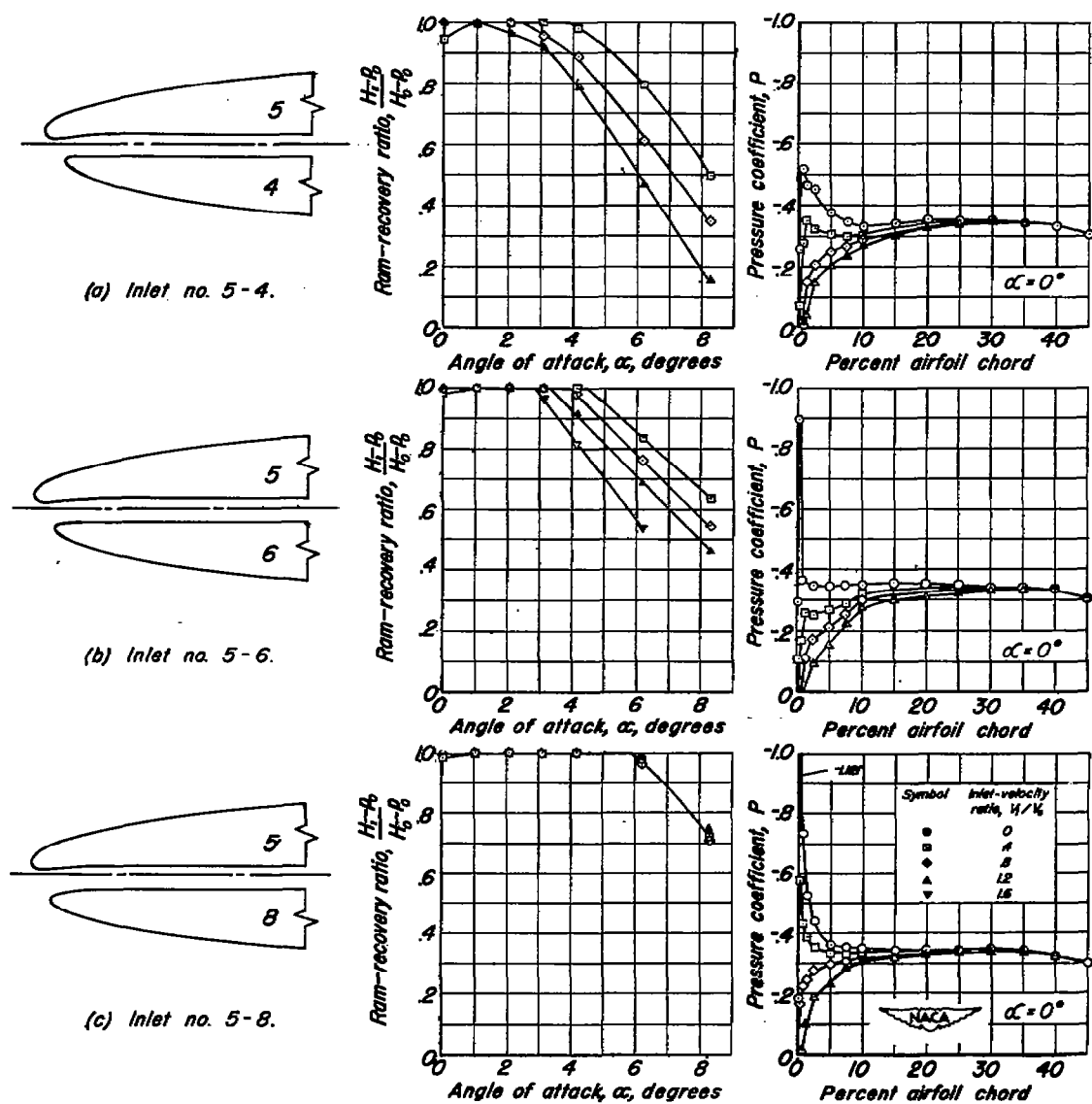


Figure 14.— Effect of change in lower-lip leading-edge shape on the ram-pressure recovery and external pressure distribution of the lower lip. Nominal  $d/t$ , 0.15 with  $20^\circ$  stagger.

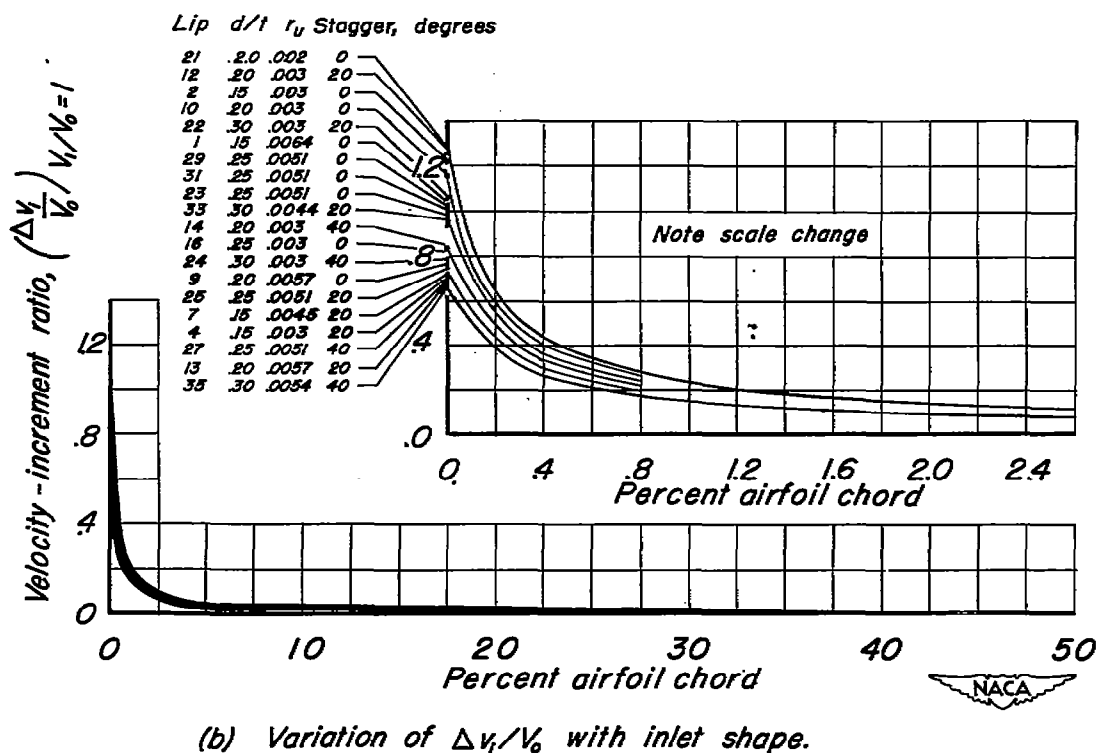
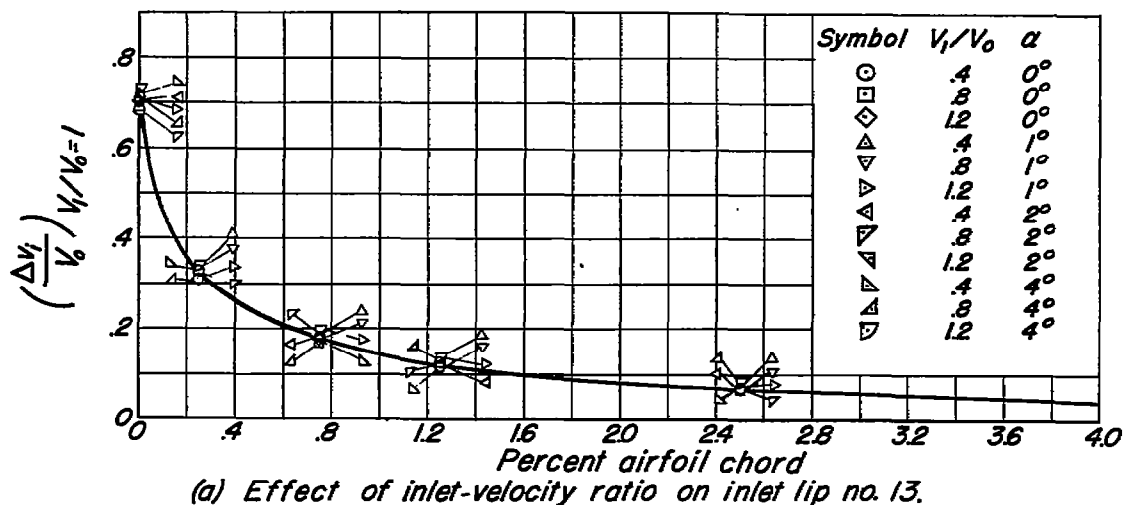
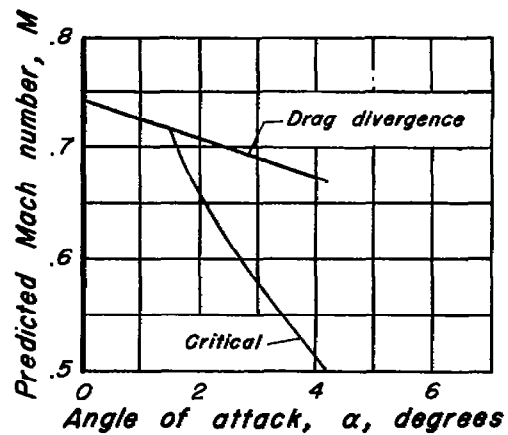
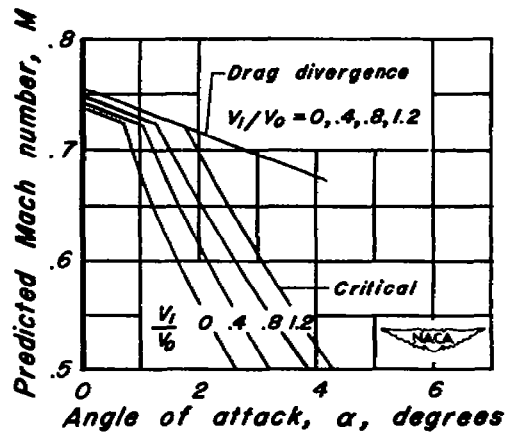


Figure 15.— Chordwise variation of velocity-increment ratio caused by inlet-velocity ratio with airfoil chord station.



(a) NACA 63-012 airfoil without inlet.



(b) NACA 63-012 airfoil with inlet no. 3-6.

Figure 16.— Predicted critical and predicted drag-divergence Mach numbers of the plain airfoil and the airfoil with design inlet number 3-6.

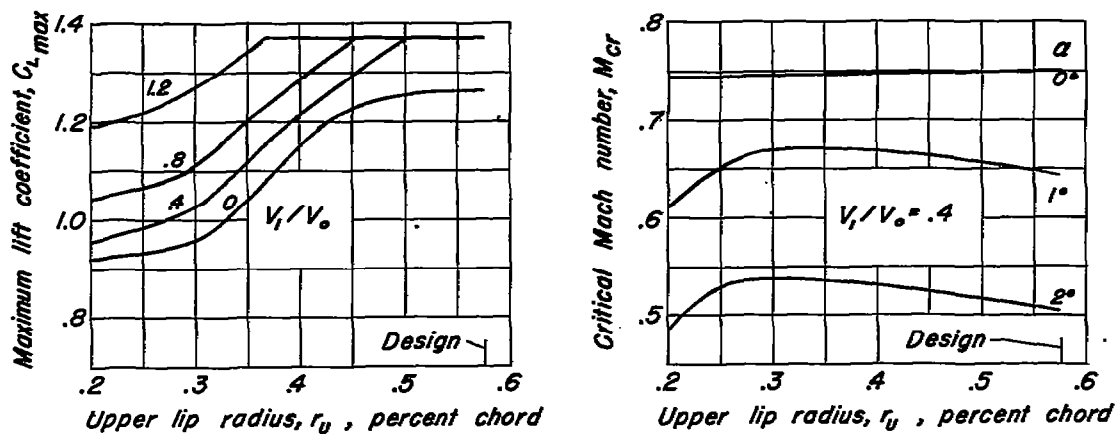
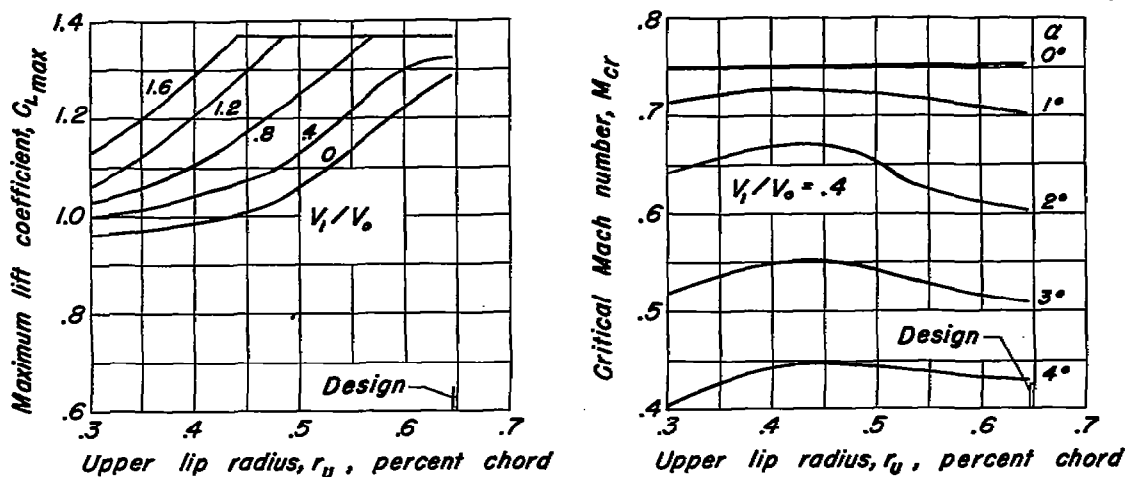
(a)  $d/t$ , 0.20 with lips unstaggered.(b)  $d/t$ , 0.15 with lips staggered  $20^\circ$ .

Figure 17.— Variation of the maximum lift coefficient and critical Mach number with upper-lip radius.

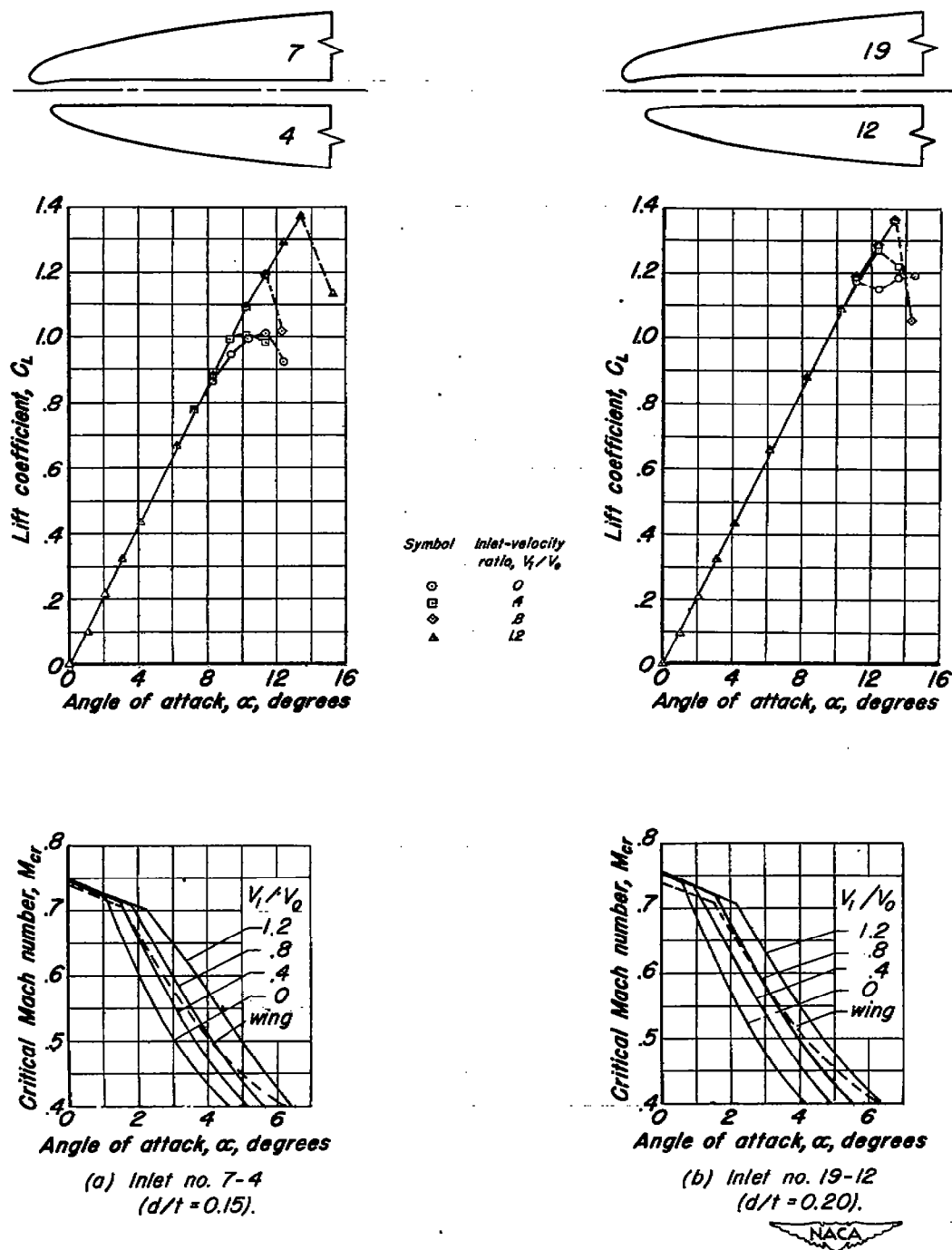


Figure 18.— General characteristics of the NACA 63-012 airfoil with modified leading-edge inlets.

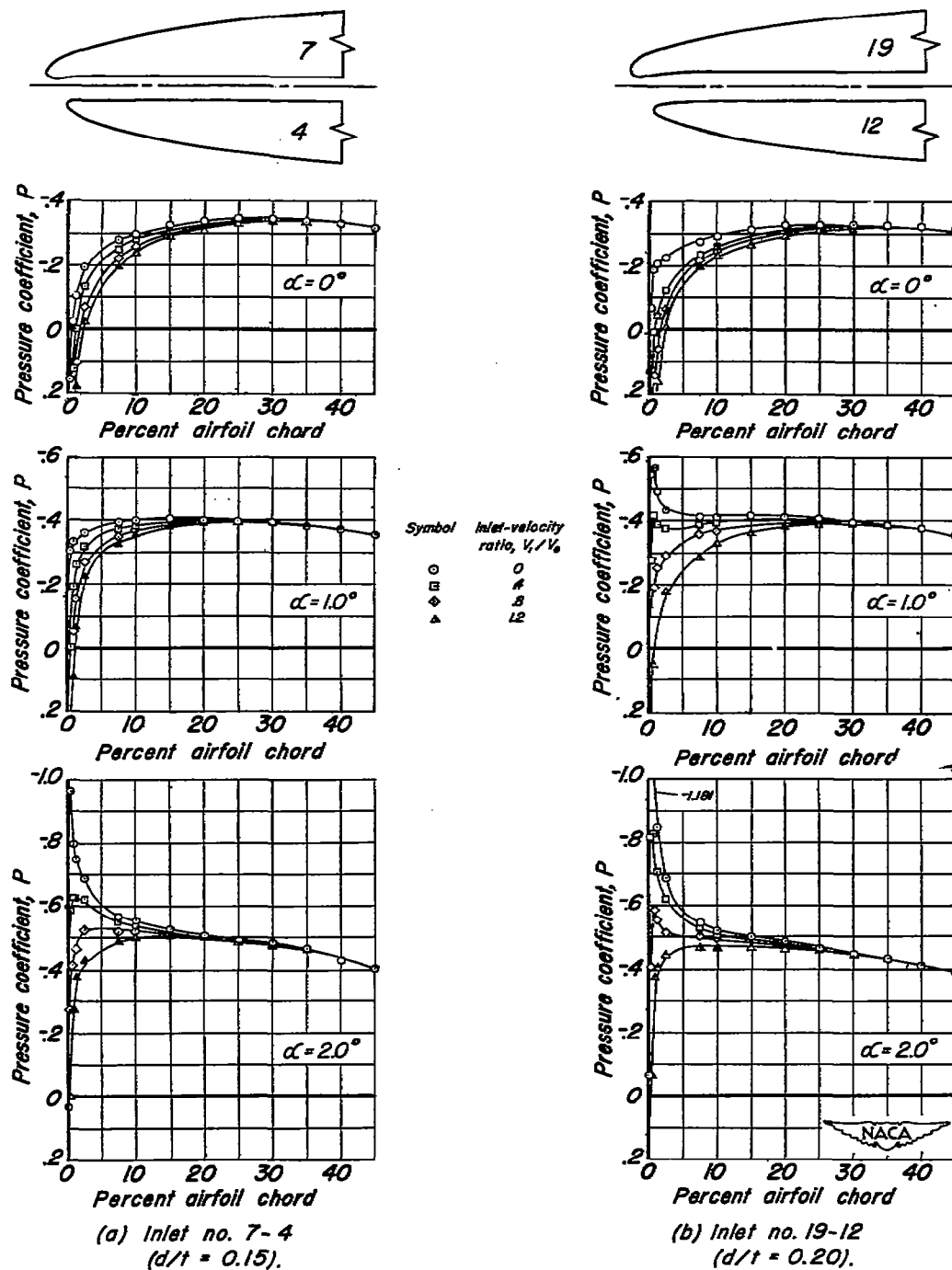


Figure 19.— External pressure distribution over the center of the upper surface of modified inlets.

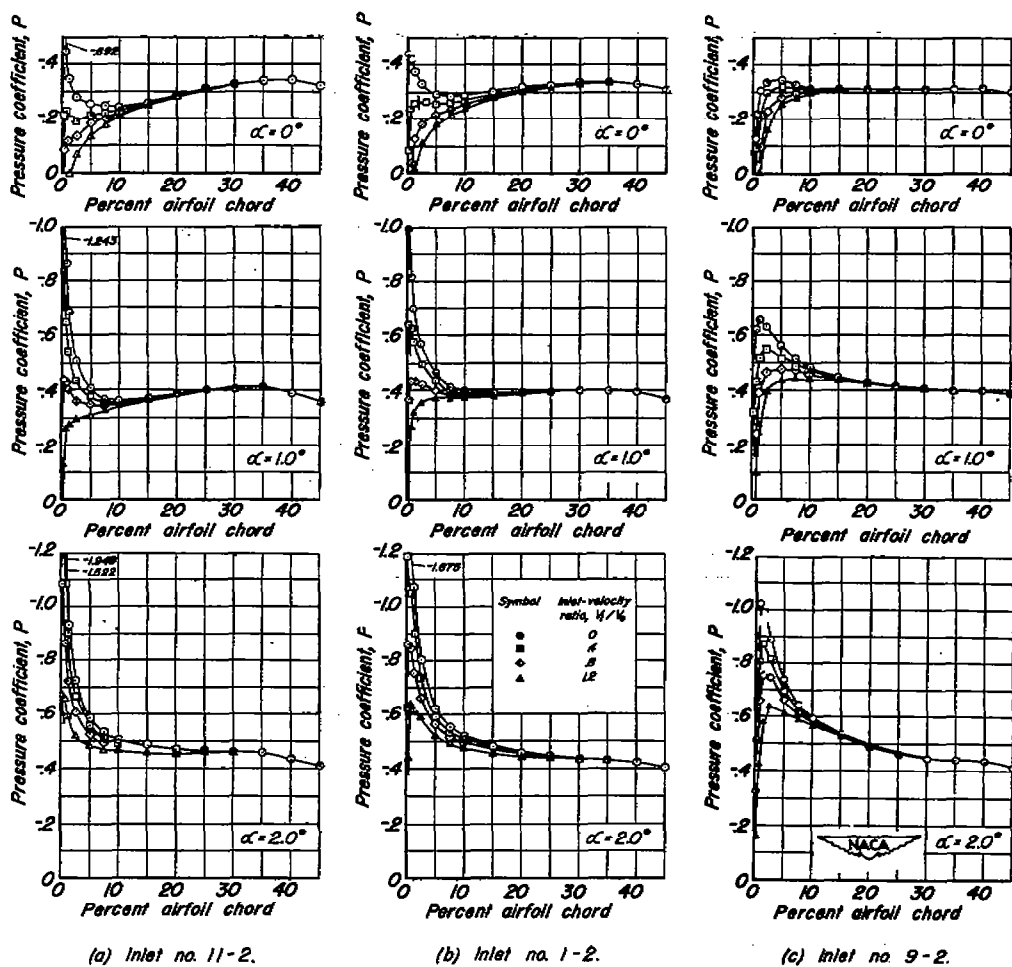
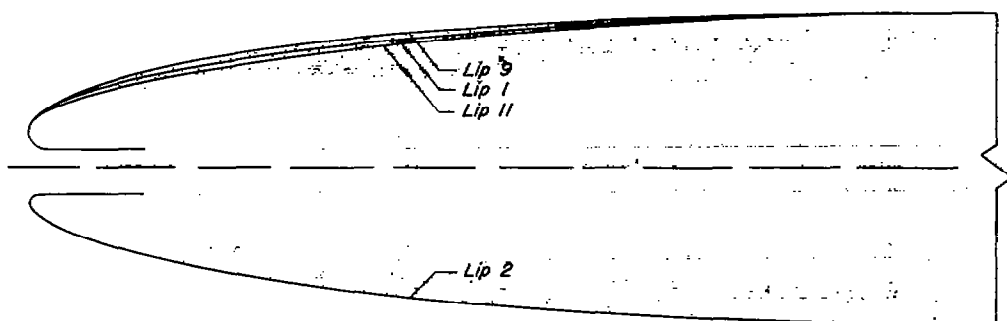


Figure 20.— Effect of changes in upper-lip external shape on the pressure distribution over the inlet section.  $d/t, 0.15$ .

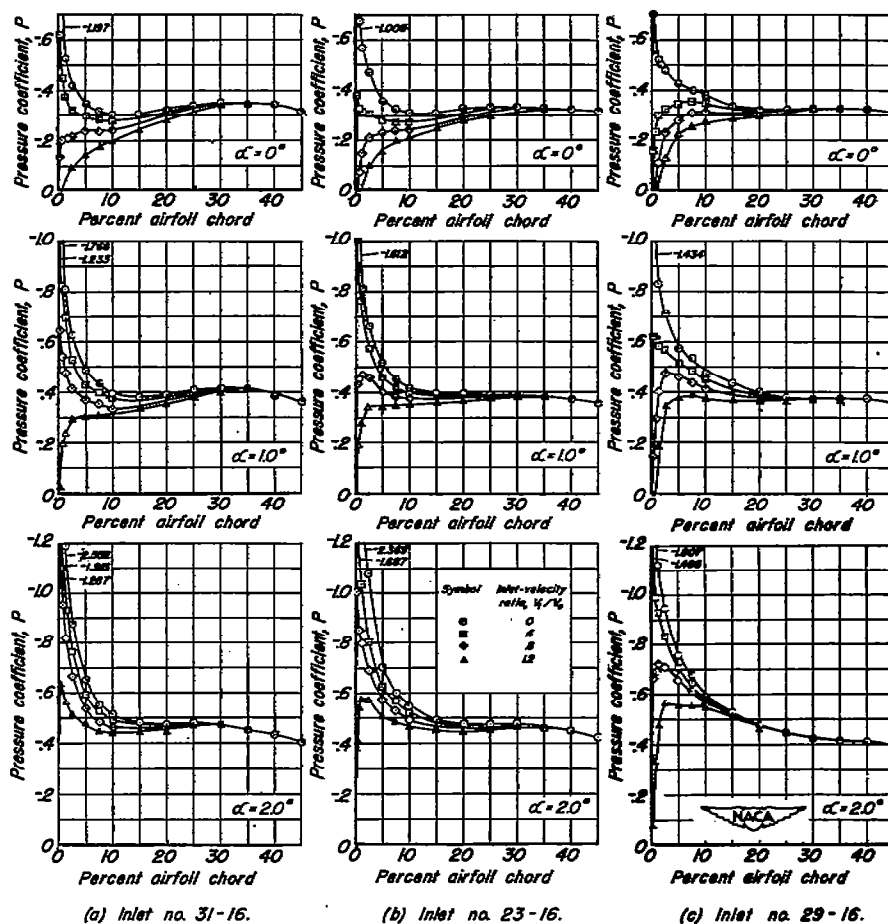
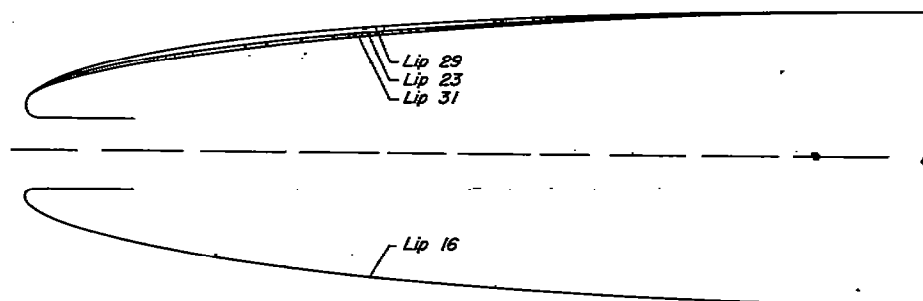


Figure 21.— Effect of changes in upper-lip external shape on the pressure distribution over the inlet section.  $d/t, 0.25$ .

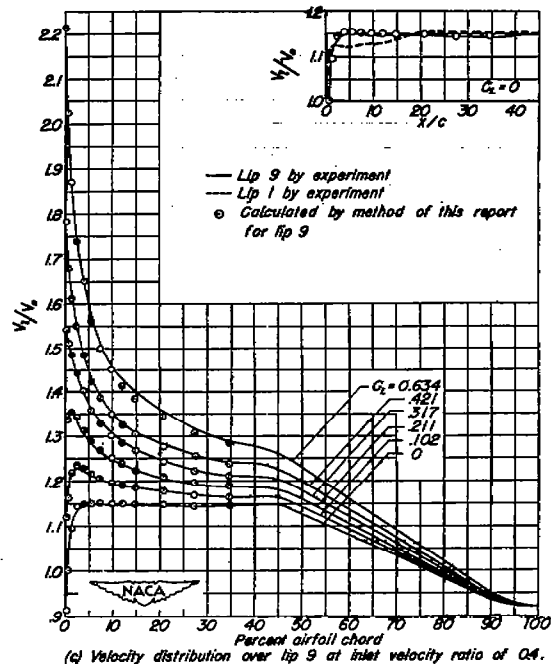
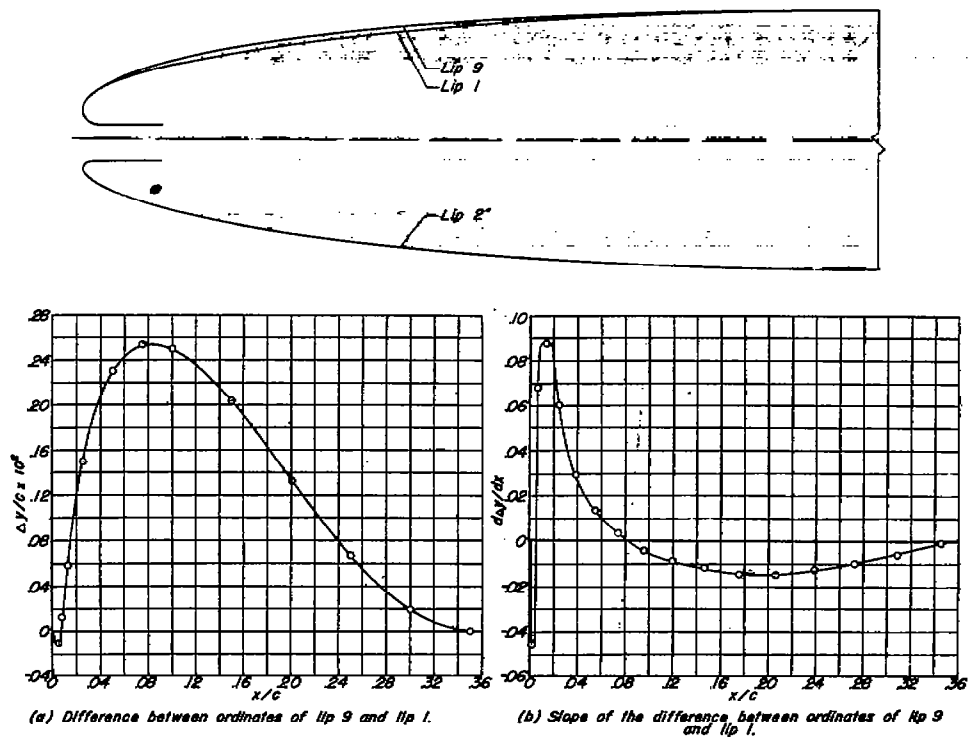
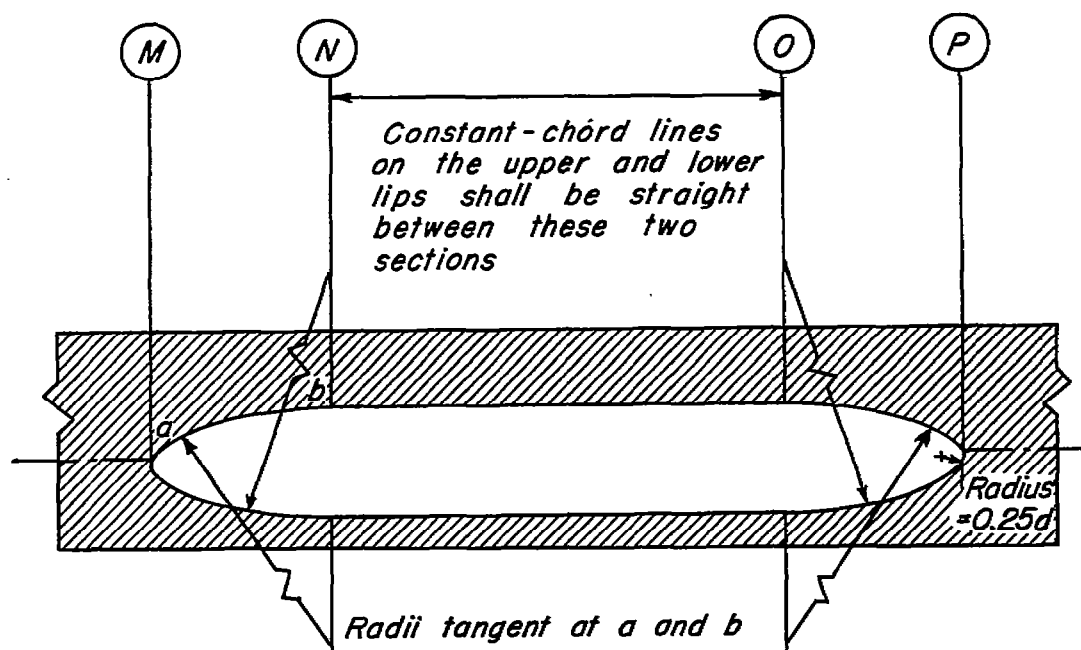
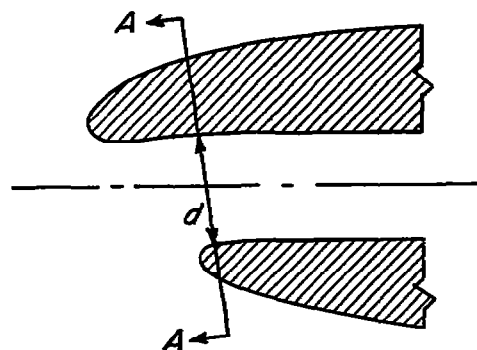


Figure 22.— Ordinate change information and calculated velocity distribution over a given leading-edge inlet.



Section A-A



Typical section from N to O



Figure 23.- End-closure shape for a design leading-edge inlet.

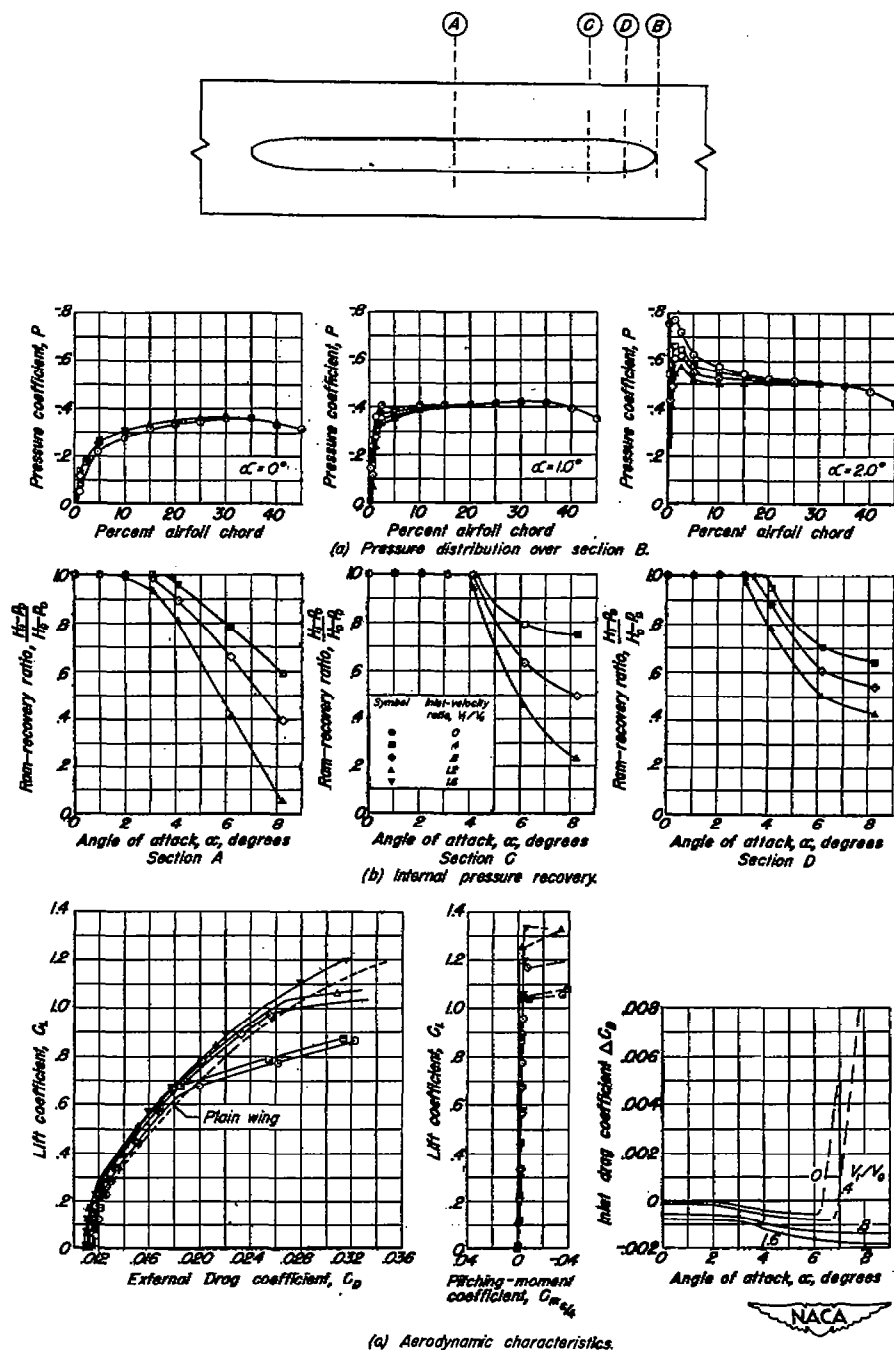


Figure 24.— General characteristics of an inlet with end-closure shape on the NACA 63,-012 airfoil.  $d/t$ , 0.20 with  $20^\circ$  stagger.

NASA Technical Library



3 1176 01425 9155